AN ABSTRACT OF THE THESIS OF

David N. Glennon for the degree of Master of Science in Electrical and Computer Engineering presented on September 19, 2019.

Title: Design and Simulation of Nonlinear Control Strategies for Heaving Point Wave Energy Converters in WEC-Sim

Abstract approved: _____

Ted K.A. Brekken

As the sources of our electricity shift from centralized and carbon emitting, to a portfolio of distributed, clean-energy sources, the wave energy converter (WEC) has become a topic of exploration and development for providing coastal communities electric power. Part of this trend has included an effort to create open source WEC modeling and simulation software. The Wave Energy Converter Simulator (WEC-Sim) provides a software solution for designing and simulating the various aspects related to wave energy, using linear wave theory and control strategies. This thesis represents a continuation of that effort and a contribution to WEC-Sim, demonstrating the use of nonlinear control strategies on wave energy converters. A fuzzy logic controller is designed and implemented in WEC-Sim, as well as a generally nonlinear control strategy for power-take-off (PTO) force. The nonlinear control models are intended for incorporation into WEC-Sim, as tutorials to

provide WEC researchers an introduction to nonlinear control methods.

Design and Simulation of Nonlinear Control Strategies for Heaving Point Wave Energy Converters in WEC-Sim

by

David N. Glennon

A THESIS

submitted to

Oregon State University

in partial fulfillment of
the requirements for the
degree of

Master of Science

Presented September 19, 2019
Commencement June 2020

Master of Science thesis of David N. Glennon presented on September 19, 2019.

APPROVED:

Major Professor, representing Electrical and Computer Engineering

---

Head of the School of Electrical Engineering and Computer Science

---

Dean of the Graduate School

I understand that my thesis will become part of the permanent collection of Oregon State University libraries. My signature below authorizes release of my thesis to any reader upon request.

David N. Glennon, Author

ACKNOWLEDGEMENTS

I would like to express my gratitude my advisor, Dr. Brekken, for his role mentoring through this project and general guidance throughout graduate school.

I would like to thank my committee members, Dr. Eduardo Cotilla-Sanchez and Dr. Bret Bosma for all your help in my learning over the past few years. A special thanks to Dr. Lewis Semprini for his availability and service as my Graduate Committee Representative.

I want to acknowledge the online WEC-Sim community, which laid the foundation for this work, as well as the Pacific Marine Energy Center for being a source of experience and knowledge.

Additionally, I must thank my cohort in the energy systems research group, for being a source of inspiration and friendship. It is a group I'm honored to be a part of.

Finally, thank you to my wife Blaire, for her continual support in my education, and my son Milo for being a constant motivation.

TABLE OF CONTENTS

TABLE OF CONTENTS (Continued)

LIST OF FIGURES

LIST OF FIGURES (Continued)

LIST OF FIGURES (Continued)

LIST OF TABLES

LIST OF APPENDIX FIGURES

Chapter 1: Introduction

As the transition to renewable sources of energy continues, the role wave energy can play in the energy mix is becoming more clear. The Electric Power Research Institute put the available wave energy resource on the outer continental shelf of the west coast of the United States at 590 TWh/yr, with at least 31% of that recoverable [1]. The high energy density in ocean waves, or incident power per unit width of wavefront, means a smaller footprint device can harvest more energy when compared to, for example, the blade-span of a wind turbine. [2] While the hurdle of renewable energy resources remains their indeterminacy, wave energy is generally more predictable and reliable. Despite these and other advantages, inhibitors to widespread investment include high capital cost of construction, maintenance costs exacerbated by corrosive seawater environments, and extreme wave events demanding design robustness to relatively rare conditions. These factors prevent rapid investment, leaving much of the industry at lower technology readiness levels (TRLs.) [3] These early stages of development have been identified as in need of critical support to encourage the adoption of wave energy converter technology [4]. Looking to the competitiveness and rapid growth of wind technology, one contributing factor is modeling software made available through United States Department of Energy (DOE) research. [5] In order to attempt to replicate the growth in the wind industry, The Wave Energy Converter Simulator (WEC-Sim) has been

developed in MATLAB. WEC-Sim is an open source code to provide numerical modeling and simulation tools to wave energy developers, thus lowering the capital barrier to designing and deploying wave energy converters. This work presents an exploration of nonlinear control strategies for power extraction in WEC-Sim.

1.1 Objective

The stated objective of the WEC-Sim project is to accelerate the pace of WEC technology development by releasing an open source, modular, WEC modeling code to meet the emerging needs of the industry and encourage a cooperative research community. [5] The objective of this thesis is to explore nonlinear methods for controlling power in WECs, and incorporate examples of these methods into WEC-Sim, so they can be reproduced and adapted, providing utility to developers. A two-level framework for nonlinear control is introduced, with a fuzzy logic supervisory control system supplying control parameters to a generally nonlinear control law. This thesis does not attempt to fully optimize or explain the generally nonlinear control law, and control parameters are determined experimentally, by data collection through simulation sweeps and exploratory optimization algorithms. While the nonlinear control law was found to be capable of providing more power than existing linear methods, to fully explain how was deemed out of scope of the intended purpose of providing wave energy researchers an introduction to and examples for well-understood nonlinear control systems.

1.2 Background

WEC-Sim v1.0 was released in December of 2015, and since that time updates and improvements have been managed through the collaboration focused software development and version control software platform GitHub.com. While requiring licenses for MATLAB, Simulink, as well as the Simscape and Multibody Simulink libraries, WEC-Sim itself is free to download and install, and has a detailed documentation website wec-sim.github.io/. Any GitHub visitor can download, use, and modify the code. Through GitHub, users can also propose changes to the code base. The project management for WEC-Sim is still funded by the DOE Water Power Technologies Office as a collaboration between the National Renewable Energy Laboratory (NREL) and Sandia National Laboratories (Sandia), which administer the GitHub repository. WEC-Sim is currently in version 3.0, with an array of tutorial models and examples in the main release, and a supplemental repository WEC-Sim_Applications containing numerous additional researcher-created demonstration models.

In order to model WEC performance, WEC-Sim uses the Simulink dynamic solver capabilities to solve the equations of motion for floating bodies. WEC-Sim is capable of employing different wave models to WEC systems composed of various physical bodies, power take-off (PTO), and Mooring systems. A high level diagram of the process is shown in Fig. 1.1 [6]. In its simplest application, a 3d model of the WEC geometry must be created (Fig. 1.1, top left) and an external boundary element method software generates the hydrodynamics coefficients of the model

geometry. Any necessary additional information and components such as the wave properties, PTO models, control models, and mooring are defined in a series of MATLAB input scripts which are called by the WecSim.m (main) function prior to running the Simulink simulation.

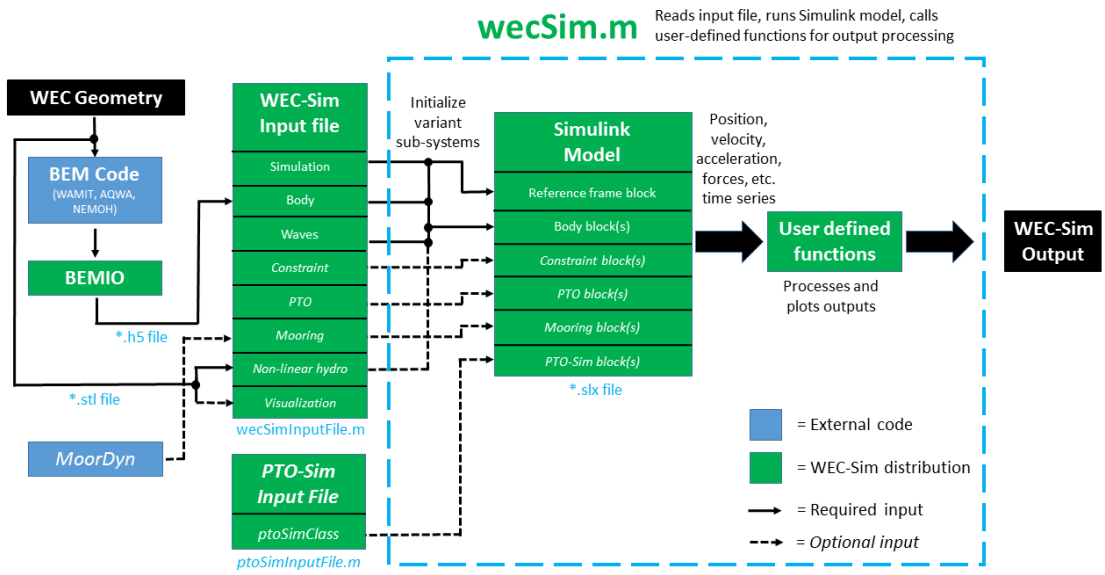

Figure 1.1: WEC-Sim workflow diagram.

The presented research is part of the Marine and Hydrokinetic Research and Development University Consortium, in a task investigating nonlinear PTO strategies in WEC-Sim. Outside of WEC-Sim, nonlinear strategies have been used on point absorber and other WEC types. Nueral networks have been used with the Archimedes Wave Swing submerged WEC to employ several control strategies [7], and a reactive control strategy based on wave period sampling for a point absorber [8]. A reactive strategy for a two-body point absorber was also implemented

using reinforcement learning [9]. A fuzzy logic controller was used to implement several control strategies for maximum power capture in a point absorber in [10]. A nonlinear passive control model for a damping coefficient was compared to a linear passive control model in [11]. A nonlinear model predictive control control methodology was applied to a point absorber with a permanent-magnet linear generator PTO [12]. The work presented in this thesis uses nonlinear fuzzy logic control to optimize power output under additional, protective, motion constraints. Additionally, a general nonlinear control law is established, and investigated, though conclusions are not drawn about the conditions which create optimal power using this control law. The next chapter details the underlying control methods for optimal power take-off of the point absorber WEC, these underlying laws are augmented by the fuzzy controller in later chapters 4 and 5, after a brief introduction to fuzzy control in Chapter 3. Conclusions are presented in Chapter 6.

Chapter 2: Control Overview

This chapter spends time developing the core control strategy for power extracted, from a passive damping control, to a linear reactive control, and a fully nonlinear control law. The example control system was applied to the RM3 model, a WEC model which is included the WEC-Sim tutorials. RM3 is a heaving point wave energy converter consisting of a floating body and a spar. A 1/100 scale model of RM3 is pictured in tank testing in Fig. 2.1 along with the tank setup in Fig. 2.2, as used in the validation of WEC-Sim [3]. In an effort to make the control system fully nonlinear, this control law was expanded to allow for nonlinear conditions, and was compared to simpler linear strategies to determine if it was possible to improve the power output of the WEC.

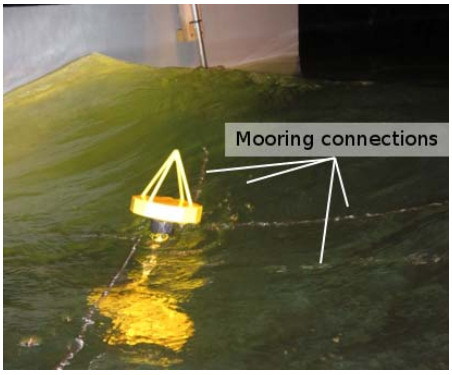

Figure 2.1: RM3 model in tank testing.

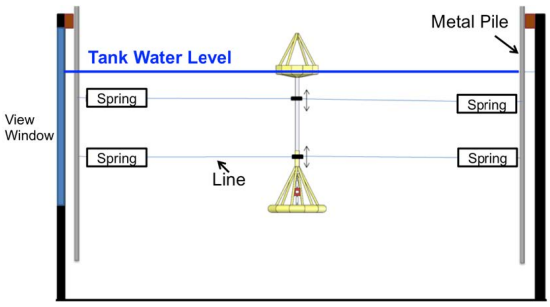

Figure 2.2: RM3 tank testing setup.

2.1 Passive Damping Control

Linear damping PTO control is often favored as a introduction for basic linear control of a heaving point absorber. For the purpose of developing the model, assume a heaving point absorber WEC, similar to RM3, is operating with a direct drive linear generator as a PTO type. The float body contains permanent magnets, which induce current in coils in the spar to generate power. Using Newton's second law an expression summing the forces acting on the WEC can be written.

$$F_e + F_r + F_h + F_{pto} = m\ddot{z} \tag{2.1}$$

Where:

- F_e is the wave excitation force on the bodies,
- F_{pto} is the force of the linear generator (or other PTO machine)
- m is the WEC mass
- $\ddot{z}$ is the relative acceleration between the bodies using the dot notation for the second time derivative of displacement, z

F_h in this expression is a result of the gravitational and buoyancy forces, referred to as the net restoring force, and is described by linear a relationship to displacement

$$F_h = -Cz \tag{2.2}$$

where C is known as the restoring stiffness, and is affected by water density, acceleration of gravity, and device geometry. F_r refers to the radiation force:

$$F_r = -A\ddot{z} - B\dot{z} \tag{2.3}$$

Where:

- A is the added mass term
- B is the mechanical resistance, referred to as radiation damping.

The radiation force is due to waves generated by the movement of the WEC body reacting with the body itself [13, pg. 125]. For the control purpose, A, B and C are hydrodynamic properties depending on the WEC geometry and wave period, and are determined by WEC-Sim as part of the simulation process. F_{pto} is the control variable, and the control objective is to maximize power take-off: P_{pto}. Assuming the PTO allows for bi-directional power flow, the generator can invest energy in the system to increase the overall average energy extracted. Substituting and arranging terms, equation 2.1 becomes the mechanical linear differential equation with constant coefficients [13, pg. 4]

$$F_e + F_{pto} = (m + A)\ddot{z} + B\dot{z} + Cz$$

Noting that in the frequency domain, the time varying $z(t)$ becomes $z(\omega)$, and that $\dot{z}$ becomes $j\omega z(\omega)$, we can write

$$F_e(\omega) + F_{pto}(\omega) = (m + A)(j\omega)^2 z(\omega) + B(j\omega)z(\omega) + Cz(\omega)$$
$$F_e(\omega) + F_{pto}(\omega) = (j(\omega(m + A) - C/\omega) + B) \cdot j\omega z(\omega)$$

For simplicity, let the intrinsic impedance of the WEC body, $Z_i(\omega)$ be defined as

$$Z_i(\omega) = j(\omega(m + A) - C/\omega) + B \tag{2.4}$$

then the relation can be written simply [14]

$$F_e(\omega) + F_{pto}(\omega) = Z_i(\omega) \cdot j\omega z(\omega) \tag{2.5}$$

using the mechanical impedance analogy which relates harmonic forces with velocities: $F(\omega) = Z(\omega)v(\omega)$. More detail about the mechanical impedance analogy is provided in Appendix B.

This intrinsic impedance is composed of a resistance component $R_i(\omega) = B$ and a reactance $X_i(\omega) = \omega(m + A) - C/\omega$, such that

$$Z_i(\omega) = R_i(\omega) + jX_i(\omega) \tag{2.6}$$

If a linear control law is selected which commands a force linearly related to and

in phase with velocity $F_{pto} = -B_{pto}\dot{z}$ the frequency domain relation becomes

$$F_e(\omega) + -B_{pto}j\omega z(\omega) = (j(\omega(m+A) - C/\omega) + B) \cdot j\omega z(\omega)$$
$$F_e(\omega) = (j(\omega(m+A) - C/\omega) + B + B_{pto}) \cdot j\omega z(\omega)$$

Which, using (2.4) and (2.5) this expression can be written

$$F_e(\omega) = (jX_i + R_i + B_{pto}) \cdot j\omega z(\omega) \tag{2.7}$$
$$F_e(\omega) = Z(\omega) \cdot \dot{z}(\omega) \tag{2.8}$$

Observe the control variable B_{pto} is able to affect the resistance portion of the system impedance, $Z = Z_i + B_{pto}$. The power transfer at the PTO generator can be written

$$P_{pto} = F_{pto}\dot{z}$$
$$P_{pto} = -B_{pto}\dot{z} \cdot \dot{z}$$
$$P_{pto} = -B_{pto}|\dot{z}|^2$$

Substituting $\dot{z} = \frac{F_e}{Z}$, from (2.7) and (2.8)

$$\begin{aligned} P_{pto} &= -B_{pto}\left|\frac{F_e}{Z}\right|^2 \\ P_{pto} &= \frac{-B_{pto}|F_e|^2}{|Z|^2} \\ P_{pto} &= \frac{-B_{pto}|F_e|^2}{|X_i + (R_i + B_{pto})|^2} \\ P_{pto} &= \frac{-B_{pto}|F_e|^2}{X_i^2 + (R_i + B_{pto})^2} \end{aligned}$$

Noting again that the components of Z_i as well as the excitation force F_e are not control variables, we differentiate P_{pto} with respect to B_{pto}, and set to 0 in order to find the extrema.

$$\begin{aligned} \frac{\partial P_{pto}}{\partial B_{pto}} &= |F_e|\left[\frac{-(X_i^2 + (R_i + B_{pto})^2) + 2B_{pto}(R_i + B_{pto}))}{(X_i^2 + (R_i + B_{pto})^2)^2}\right] \\ 0 &= |F_e|\left[\frac{-(X_i^2 + (R_i + B_{pto})^2) + 2B_{pto}(R_i + B_{pto}))}{(X_i^2 + (R_i + B_{pto})^2)^2}\right] \\ 0 &= \left[-(X_i^2 + (R_i + B_{pto})^2) + 2B_{pto}(R_i + B_{pto}))\right] \\ B_{pto}^2 &= X_i^2 + R_i^2 \\ B_{pto} &= \sqrt{R_i^2 + X_i^2} \end{aligned}$$

Recalling $Z_i = R_i + jX_i = B + j(\omega(m + A) - C/\omega)$, power is maximized under the

passive damping strategy when

$$B_{pto} = \sqrt{(\omega(m+A) - C/\omega)^2 + B^2}$$
$$B_{pto} = |Z_i|$$

2.2 Reactive Control

As noted, in the passive damping strategy the PTO generator does not handle reactive power, such as the mechanical power related to forces of buoyancy and inertia (refer to Appendix B for a complete description of the mechanical impedance analogy). If we instead define the control law

$$F_{pto} = -B_{pto}\dot{z} - C_{pto}z \tag{2.9}$$

the expression for the excitation force becomes

$$F_e = (j(\omega(m+A) - 1/\omega(C + C_{pto})) + B + B_{pto}) \cdot j\omega z(\omega) \tag{2.10}$$

where the PTO impedance is positioned to also affect the reactance portion of the intrinsic impedance. That is

$$
\begin{aligned}
F_e &= Z \cdot \dot{z} \\
F_e &= (Z_i + Z_{pto}) \cdot \dot{z} \\
F_e &= (R_i + R_{pto} + j(X_i + X_{pto})) \cdot \dot{z} \\
F_e &= (j(\omega(m + A) - 1/\omega(C + C_{pto})) + B + B_{pto}) \cdot \dot{z}
\end{aligned}
$$

Where the PTO impedance has been defined

$$
\begin{aligned}
Z_{pto} &= R_{pto} + jX_{pto} \\
&= B_{pto} - jC_{pto}/\omega
\end{aligned}
$$

As in electronics, the maximum useful power transfer will occur when the load impedance magnitude is matched and complex portions are canceled by the conjugate: $Z_i + Z_{pto} = 2\,\mathrm{Re}\{Z_i\}$, [13, pg. 202] or

$$
\begin{aligned}
R_{pto} &= R_i \\
R_{pto} &= B \\
B_{pto} &= B
\end{aligned}
\tag{2.11}
$$

and,

$$\begin{aligned} X_i + X_{pto} &= 0 \\ (\omega(m+A) - C/\omega) - (C_{pto}/\omega) &= 0 \\ C_{pto}/\omega &= \omega(m+A) - \frac{C}{\omega} \\ C_{pto} &= \omega^2(m+A) - C \end{aligned} \tag{2.12}$$

Under this condition the reactive component of the impedance, representing wasted energy exchanged via the mass and restoring stiffness, are cancelled. Despite the analogy to impedance matching in electronic circuits, this is sometimes called complex conjugate control, or reactive control when applied to wave energy converters [15] [16]. Note that not all negative values for C_{pto} will produce a stable result. The stability limit for this term is explained further in Appendix C.

2.3 Nonlinear Control

Reviewing the control law, $F_{pto} = -B_{pto}\dot{z} - C_{pto}z$ it is evident that this meets the definition of a linear control law: the control variable F_{pto} is dependent on linear polynomial combinations of z and its orders of time derivative. To generalize this linear case to a nonlinear law, control variables for the exponents of $\dot{z}$ and z can be added, the general rule becomes:

$$F_{pto} = -B_{pto} \cdot \text{sign}(\dot{z}) \cdot |\dot{z}|^{\alpha} - C_{pto} \cdot \text{sign}(z) \cdot |z|^{\beta} \tag{2.13}$$

where the sign of $\dot{z}$ and z have been accounted for to prevent even numbered exponents reversing motion in the negative direction. Determining the maximum power condition presents a 4 dimensional optimization problem, where we would like to maximize power given the freedom to vary the impedance coefficients as well as the powers of position and velocity. In order to investigate this control strategy, several methods were employed to determine the optimal parameters experimentally in WEC-Sim.

2.3.1 Parameter Sweeps

Initial attempts to define the control space involved sweeping each of the 4 parameters. The impedance values were swept through values in the neighborhood of their optimum values for the reactive control strategy, and the exponents were swept through values near 1. This was done under a series of sea states in an attempt to map the surface and try to establish some patterns with respect to power. Since a selection of plausible waveheights and average periods were also being swept, simulating even a low resolution in each parameter became a prohibitively long computation time, for example, even just 3 values for each parameter results in $3^6 = 729$ simulations in WEC-Sim. One outcome of this strategy was that the waveheight, while affecting the total power output, did not influence the selection of the optimal parameters as much as wave period. This was expected based on the parameter's relationship to period in the linear reactive control law.

2.3.2 Simple Hill Climbing

The brute force sweep approach was exchanged for a more sophisticated random-walk hill-climbing algorithm. A simplified flowchart for this algorithm is shown in Fig. 2.3. While it did not travel the path of steepest gradient to the maximum power, this algorithm was used for its speed of implementation. Several design decisions for the algorithm were unclear. The random increments to the parameters were determined from a Gaussian random variable, which had a standard deviation of 5% of the current value of the variable. For example, if for an iteration i,

$$B_{pto}(i) = 100$$

the next iteration would be determined by

$$B_{pto}(i+1) = 100 + \mathrm{N}(\mu = 0, \sigma^2 = 25)$$

The algorithm's success is highly sensitive to this increment size, which represents a key design trade-off. If too small an increment is used, the time to converge to a maxima would be too long, since each increment involves a WEC-Sim model simulation. However, too large an increment might cause the algorithm to overstep the maxima, decreasing accuracy and converging far from an optimal value. Another unclear parameter is the number of iterations required without a new solution before the algorithm exits. Since there are four variables randomly incrementing, this number of iterations must be sufficient to give a high probability that a step

in every direction was tried, 16 possible step directions, without finding a point which produced more power. Finally, this algorithm is sensitive to local extrema, and in order to overcome this, it would need to be initialized with different starting points to ensure the space was thoroughly explored, significantly increasing the total computation time. There are programming options to address these drawbacks, such as lowering the step size as the number of iterations without a new solution increases, and occasionally trying much larger steps to try to shake the algorithm out of local maxima. However, it was decided that making these improvements might confound the real goal of exploring nonlinear control strategies. For this reason a more off-the-shelf optimization solution was sought.

2.3.3 Parameter Optimization Using fmincon

While improvements could have been made to the hill climbing algorithm, it was abandoned in favor of MATLAB's Optimization Toolbox, specifically the fmincon function for constrained optimization problems. Constrained optimization seeks the minimum of a function for a given vector of inputs, and a set of constraints on the inputs. The fmincon function represents a set of optimization algorithms, the Interior Point Algorithm was specifically used for this problem. The Interior Point Algorithm is recommended for general cases in fmincon, due to handling both sparse and dense problems. It is a large-scale algorithm, performing linear algebra computations quickly and using less memory than alternatives. The interior point approach attempts to solve a sequence of easier to solve approximate minimizations

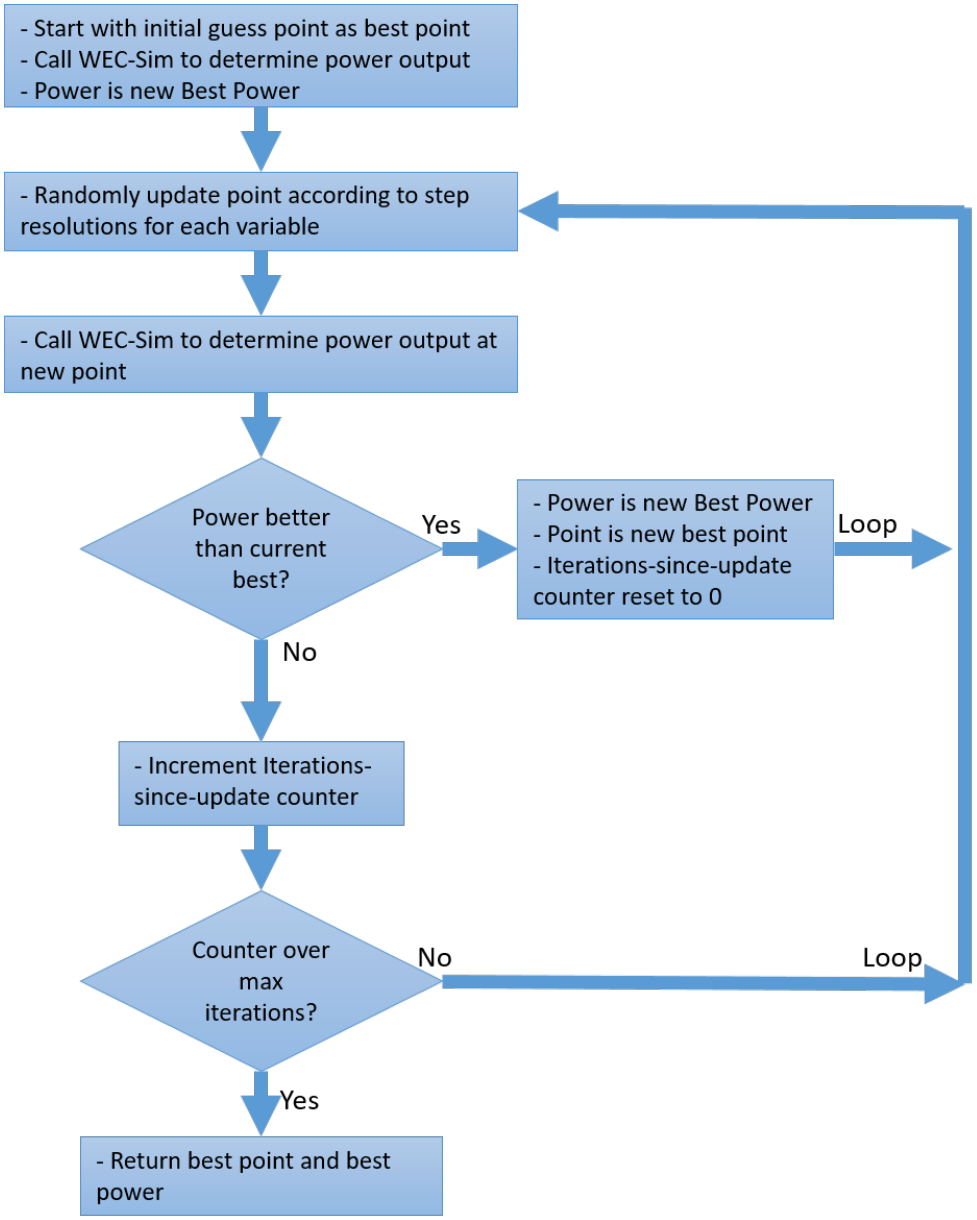

Figure 2.3: A flowchart for the random walk algorithm used to find the optimal B_{pto}, C_{pto}, α, and β parameters for the nonlinear control law.

of the objective function [17] [18] [19].

A flowchart of the script which employed fmincon to optimize the power output over a series of wave conditions is shown in Fig. 2.4. By repeatedly calling WEC-Sim, modifying parameters based on the results and constraints, the algorithm sought to find the set of damping, stiffness, and exponents for velocity and position which produced the minimum power[1] for a given sea state. The constraints for the optimization initially limited the exponents to between one and three, to limit simulation time. B_{pto} was initially allowed a large range, several times the range of values used in the reactive damping strategy, since there were no stability concerns. Eventually the limits for B_{pto} were tightened to reduce the simulation time, since they were not converging in the extreme values. Stiffness was more difficult to select limits for, since too negative a value could affect the control system's stability. Initially, the limit was set to the same limit as was used for reactive damping. That lower limit was sufficient for most sea states to converge, and was the final value for many of the tested conditions. The final parameters for a range of sea states is shown in table 2.1, along with the respective parameters and optimal power using the other strategies.

2.3.4 Output Power Comparison

A summary of the control parameters used for each strategy is shown in table 2.1, across a range of regular wave periods and heights. The B_{pto} and C_{pto} parameters

[1] where power extracted is defined as negative, thus the minimum represents most power captured

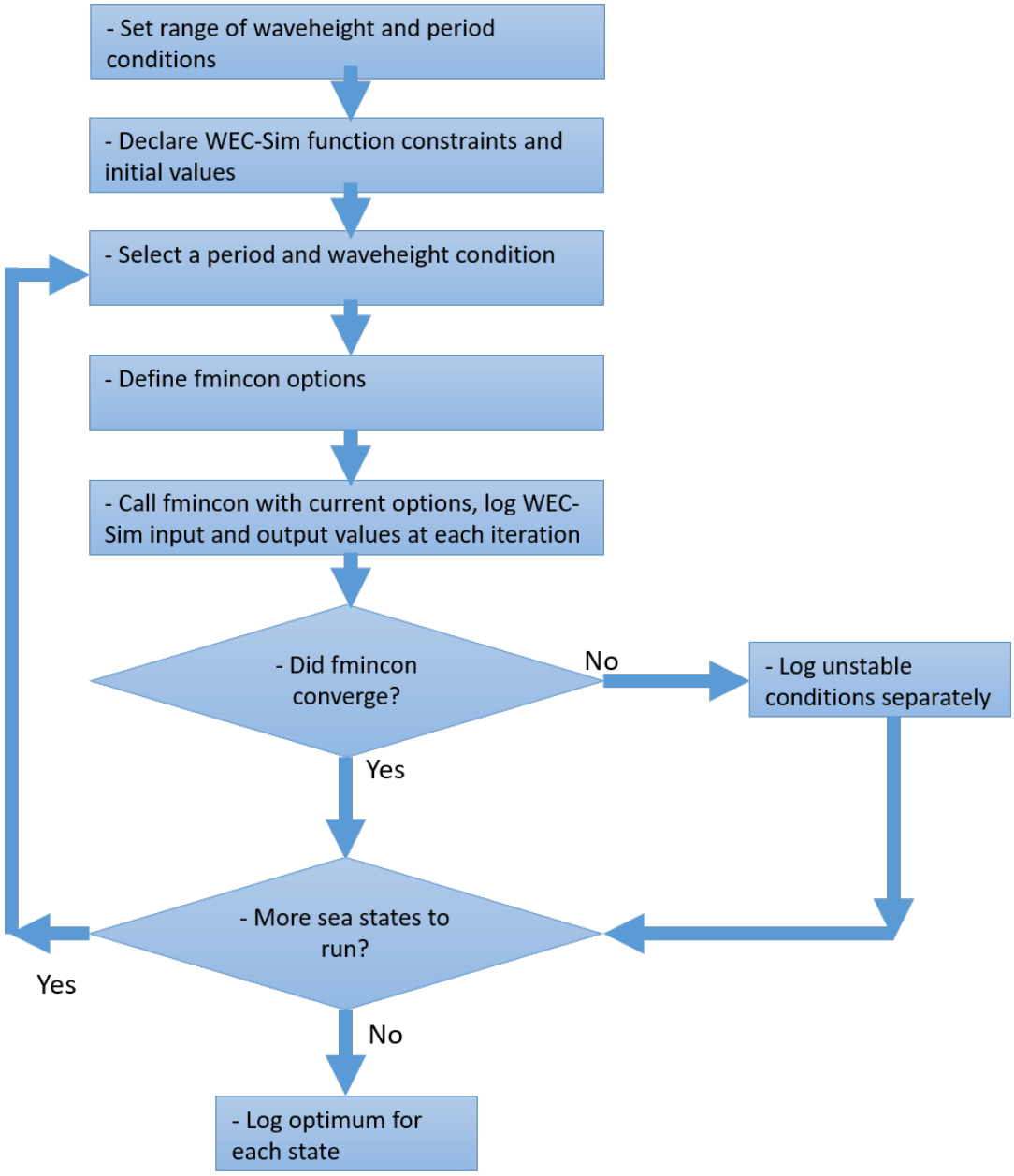

Figure 2.4: Flowchart for script using fmincon with WEC-Sim's power output as an objective function.

used in passive damping and reactive strategies were calculated using the point absorber's intrinsic impedance at the given period, as described in Appendix B. The B_{pto}, C_{pto}, α, and β parameters used in the nonlinear strategy were determined by fmincon. A graphical comparison of the PTO power is shown in Fig. 2.5. Using fmincon to optimize the nonlinear control law was able to achieve an average 11% improvement in power captured over the passive damping strategy.

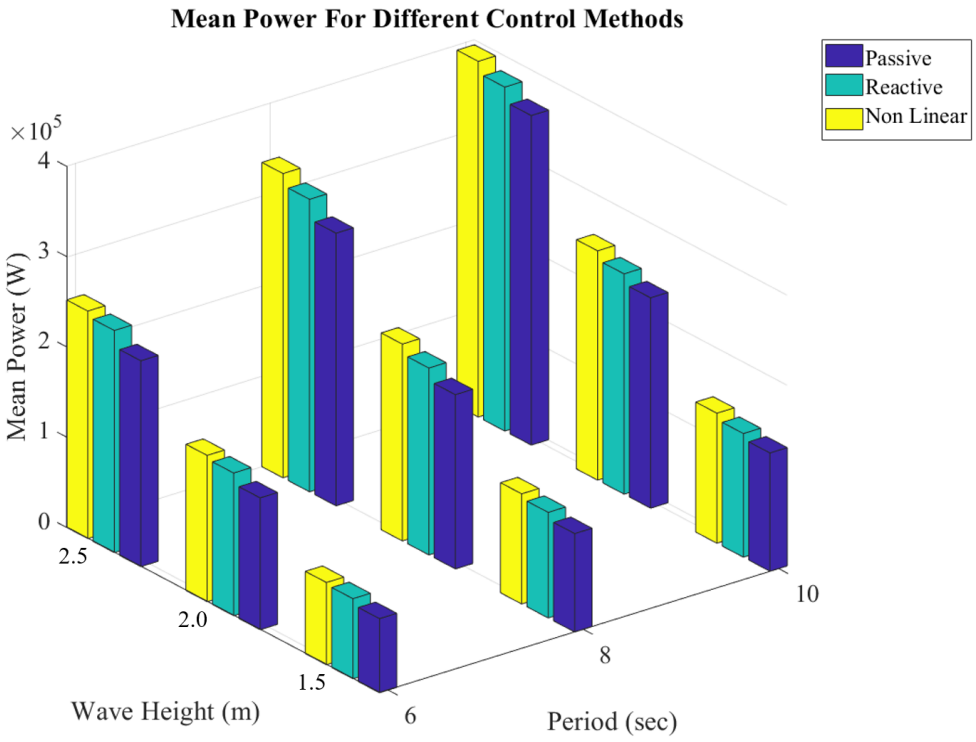

Figure 2.5: Comparison of power take-off at the optimal parameters for the control strategies described in Chapter 2.

Control	**T (s)**	**H (m)**	B_{pto}	C_{pto}	α	β	**Avg PTO (W)**	**Gain**
Passive	6	1.5	1.02E+06				8.21E+04	1
		2	1.02E+06				1.46E+05	1
		2.5	1.02E+06				2.28E+05	1
	8	1.5	2.59E+06				1.09E+05	1
		2	2.59E+06				1.93E+05	1
		2.5	2.59E+06				3.02E+05	1
	10	1.5	5.92E+06				1.31E+05	1
		2	5.92E+06				2.33E+05	1
		2.5	5.92E+06				3.65E+05	1
Reactive	6	1.5	8.90E+05	-2.25E+05			8.87E+04	1.08
		2	8.90E+05	-2.25E+05			1.58E+05	1.08
		2.5	8.90E+05	-2.25E+05			2.46E+05	1.08
	8	1.5	2.33E+06	-2.25E+05			1.17E+05	1.07
		2	2.33E+06	-2.25E+05			2.07E+05	1.07
		2.5	2.33E+06	-2.25E+05			3.24E+05	1.07
	10	1.5	5.58E+06	-2.25E+05			1.37E+05	1.04
		2	5.58E+06	-2.25E+05			2.44E+05	1.04
		2.5	5.58E+06	-2.25E+05			3.81E+05	1.04
Nonlinear	6	1.5	9.37E+05	-2.24E+05	1.04	0.66	9.11E+04	1.11
		2	7.78E+05	-2.25E+05	0.82	0.49	1.62E+05	1.11
		2.5	7.44E+05	-2.25E+05	0.59	0.39	2.52E+05	1.10
	8	1.5	1.41E+06	-2.20E+05	0.62	0.50	1.22E+05	1.13
		2	1.58E+06	-2.25E+05	0.62	0.39	2.18E+05	1.13
		2.5	1.76E+06	-2.25E+05	0.62	0.36	3.37E+05	1.12
	10	1.5	3.12E+06	-2.25E+05	0.66	0.38	1.44E+05	1.10
		2	3.60E+06	-2.25E+05	0.69	0.37	2.54E+05	1.09
		2.5	3.83E+06	-2.25E+05	0.65	0.31	3.94E+05	1.08

Table 2.1: Optimal parameters for the various control strategies described in Chapter 2, and the respective optimal power, also shown in Fig. 2.5. Parameters for the nonlinear control law in equation 2.13 were determined by fmincon. Gain is calculated with respect to the passive damping strategy.

Chapter 3: Overview: Fuzzy Control Systems

This chapter briefly sets aside the topic of wave energy converters to give a general explanation of fuzzy logic control. Fuzzy logic is paradigm which allows for a linguistic and intuitive design of control systems. Fuzzy logic is classified with multi-valued logic systems. In contrast with the typical digital binary of true and false, in multi-valued logic, truth may take on an analog value between totally false, zero, and totally true, one. Because of this, a fuzzy system input's classification becomes imprecise, and control laws can be described using basic language in a way which still encompasses the range of a control space. This section gives an overview of the components and process of fuzzy systems, using a simple control example: controlling home room temperature using a temperature sensor to set fan speed.

3.1 Fuzzy Concepts: Sets, Membership, Rules

A simplified diagram of a fuzzy logic controller is shown in Fig. 3.1. The inputs of a fuzzy system are crisp quantitative values, such as temperature measurements from a sensor. Fuzzy sets are descriptive groups of the possible values of an input, where a given input value may be a partial member of more than one set. For example, the set of indoor temperatures considered *warm* may range from 82 to 85

degrees Fahrenheit, while *hot* is a temperature above 90 degrees Fahrenheit. The in-between temperature of 88°F may belong to both sets, considered for instance, 60% (0.6) a member of *hot* and 40% (0.4) *warm*[1].

For every fuzzy temperature set, every allowed temperature value across the input range can be assigned a level of membership truth between zero and one. These values are assigned based on a membership function (MF) defined for each set, which plots the membership truth across the input range. The membership function for the example definition of *warm* is shown in Fig. 3.2. Expanding the example, input temperature may be defined across a range of possible values from 64-100°F, and membership functions for *cold* and *comfortable* are added, as in Fig. 3.3. Both *cold* and *comfortable* would evaluate a 0% membership for the previous input of 88°F. Similarly, fuzzy sets and corresponding membership functions are defined for the output variables, such as, if the output for the example control system is the rotational speed of a fan blowing cold air, the RPM fuzzy sets' membership functions may be defined as shown in Fig. 3.4.

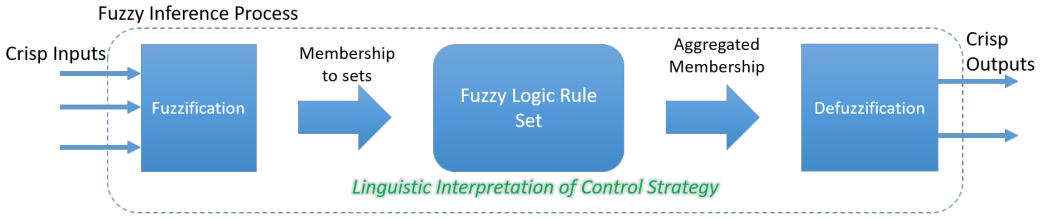

Figure 3.1: General flow chart of the fuzzy inference process.

[1]Hereinafter, descriptor words will be *italicized* when they refer to a specifically defined fuzzy set, as opposed to the colloquial meaning.

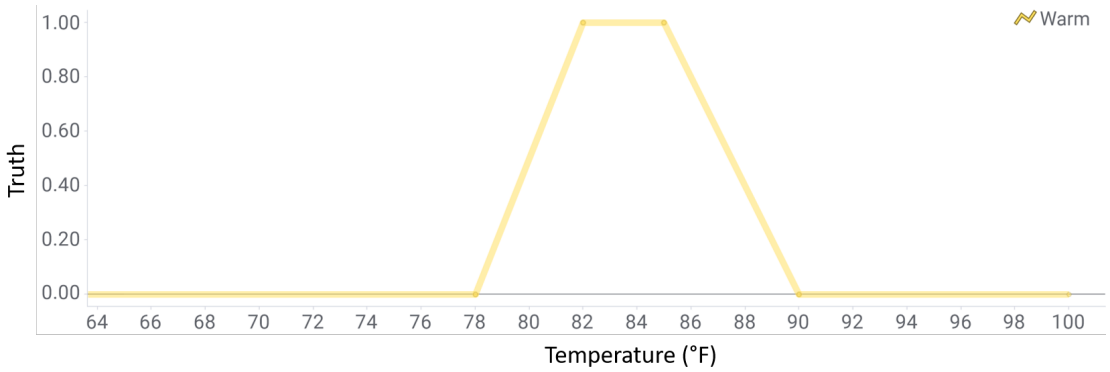

Figure 3.2: Membership function for warm temperatures.

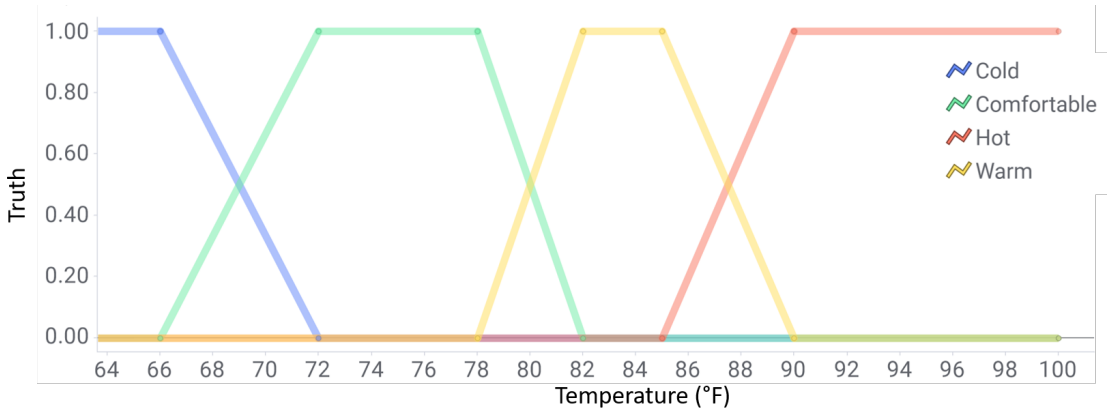

Figure 3.3: Membership functions for full temperature input allowed range.

While thus far this process may seem contrived and somewhat arbitrary, it provides a means for a computer to interpret a set of linguistic if-then rules which are also easy to understand for human operators. The set of rules which could define this example control system is:

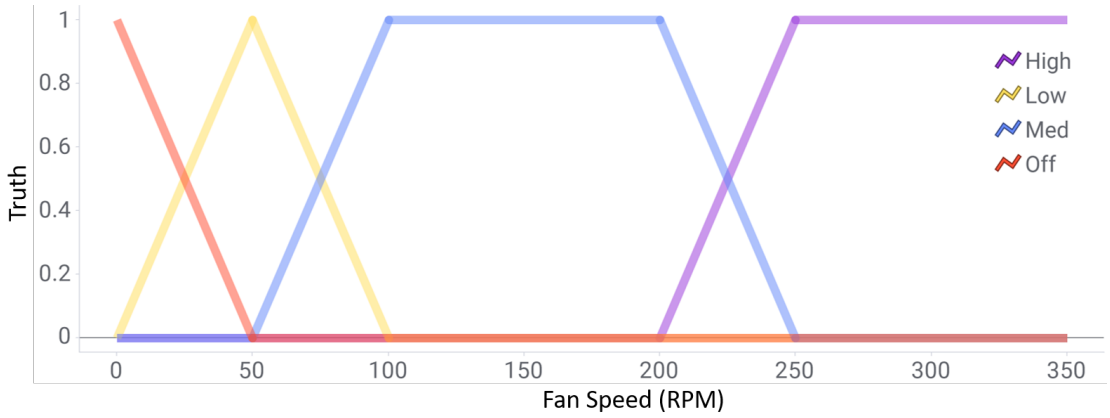

Figure 3.4: Membership functions for a fan speed output.

1. If temperature is *hot*, then fan speed is *high*.
2. If temperature is *warm*, then fan speed is *medium*.
3. If temperature is *comfortable*, then fan speed is *low*.
4. If temperature is *cold*, then fan speed is *off*.

The "If" portion of each rule is referred to as the antecedent, it is a conditional clause corresponding to one or more of the input fuzzy sets. The "then" portion is called the consequent, it is a clause related to a fuzzy set of an output. Note that multiple rules may correspond to the same output set, for example multiple rules may result in seting the fan speed to *medium*.

3.2 Fuzzy Inference Process

A fuzzy logic controller evaluates its inputs according to their membership functions and determines the output based on these if-then rules. This is called the

fuzzy inference process, and has the following steps:

1. Fuzzify System Inputs
2. Apply Fuzzy Operators
3. Rule Weighting
4. Apply Implication Method
5. Aggregate Rules
6. Defuzzify System Outputs

the remainder of this section details these steps and some of their options, maintaining the example system and instantaneous input of 88°F.

1. Fuzzification is the process described above by which the crisp system input values are passed to a series of membership functions and assigned a truth value for each one: it is the process by which 88°F is interpreted as 0% *cold*, 0% *comfortable*, 40% *warm* and 60% *hot*. In this example, and many applications, it is a matter of design decision where the exact boundaries of the partial member ranges are. However, there is value in selecting them according to a general trend that would be widely agreed upon for the given context. In particular, the membership ranges should be agreed upon by those who would be operating or interacting with the system, to ensure its operation is understood.

2. The application of fuzzy operators to the inputs is not always a necessary step; it is only required for system rules which have more than one input. Suppose a second input to the example system is created, for a schedule of times for which the fan does not need to operate as the occupants are away. The membership function for the single *away* set is shown in Fig. 3.5, and corre-

sponds to a typical working hours, with fuzzy edges. Rule 4 is modified to state

4. If temperature is *cold* OR schedule is *away,* then fan speed is *off*.

Now the logical operator OR needs to be clarified. In typical digital logic, a clear truth table exists for the OR operator, however for the multi-valued logic used in fuzzy systems there are potentially infinitely many input combinations. To produce a similar effect of the digital OR, a MAX (maximum) function can be used to resolve the conditional. The antecedent will evaluate to completely true if either input is completely true. In the case neither are fully true, the highest partially true value is selected, regardless if other inputs are completely false, which is also in accordance with the digital OR. Similarly, a fuzzy AND can be accomplished with the MIN (minimum) function, resolving to false if any input is completely false, or resolving to the most false partial value. Depending on the application, a number different fuzzy operators might be used to resolve a rule's antecedent to a single analog truth value. This is referred to as the rule antecedent truth, or rule firing strength, and is required for the next steps in the fuzzy inference process.

3. In the case there is more than one rule affecting the same set, or same output, it is possible to reduce the influence of some rules by assigning a rule weight less than one. If a weighting less than one were assigned, the weighting would simply be multiplied by the firing strength, reducing the rule's impact on the later aggregation step. The outcome of the weighting step is a single analog truth value for the antecedent of each rule, now modified by the rule weight. This is an optional step, and is disregarded for the fuzzy systems presented in this work: all rules are weighted equally to the default value of 1, and so this step is not

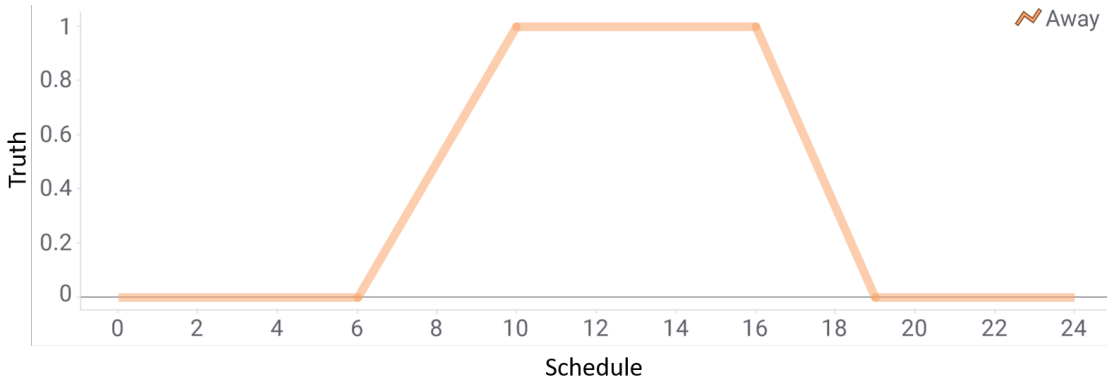

Figure 3.5: Additional input for the example system indicating the fan does not need to operate from the hours of 10 to 17, with partial membership as early as 6 and late as 19.

shown.

4. The output membership function for *medium* shown in Fig. 3.4 gives the truth for each output value when the conditions of the antecedent are completely true, or 1. If the antecedent is partially true, what does that *imply* about the output membership function? The antecedent value is used to shape the output membership function, using an implication method. Two common methods are to take the product of the firing strength and the output membership function, scaling the function, or to take the minimum of both, clipping the membership function. For the example input of 88°F, the result of both of these methods on the *medium* output membership function (*warm* antecedent = 0.4) is shown in Fig. 3.6. The result of this step is a collection of membership functions, each representing a fuzzy set found in the consequent of a rule, referred to as a consequent membership function. Note that a given output fuzzy set may have more than one consequent

membership function, if it appears in the consequent of more than one rule.

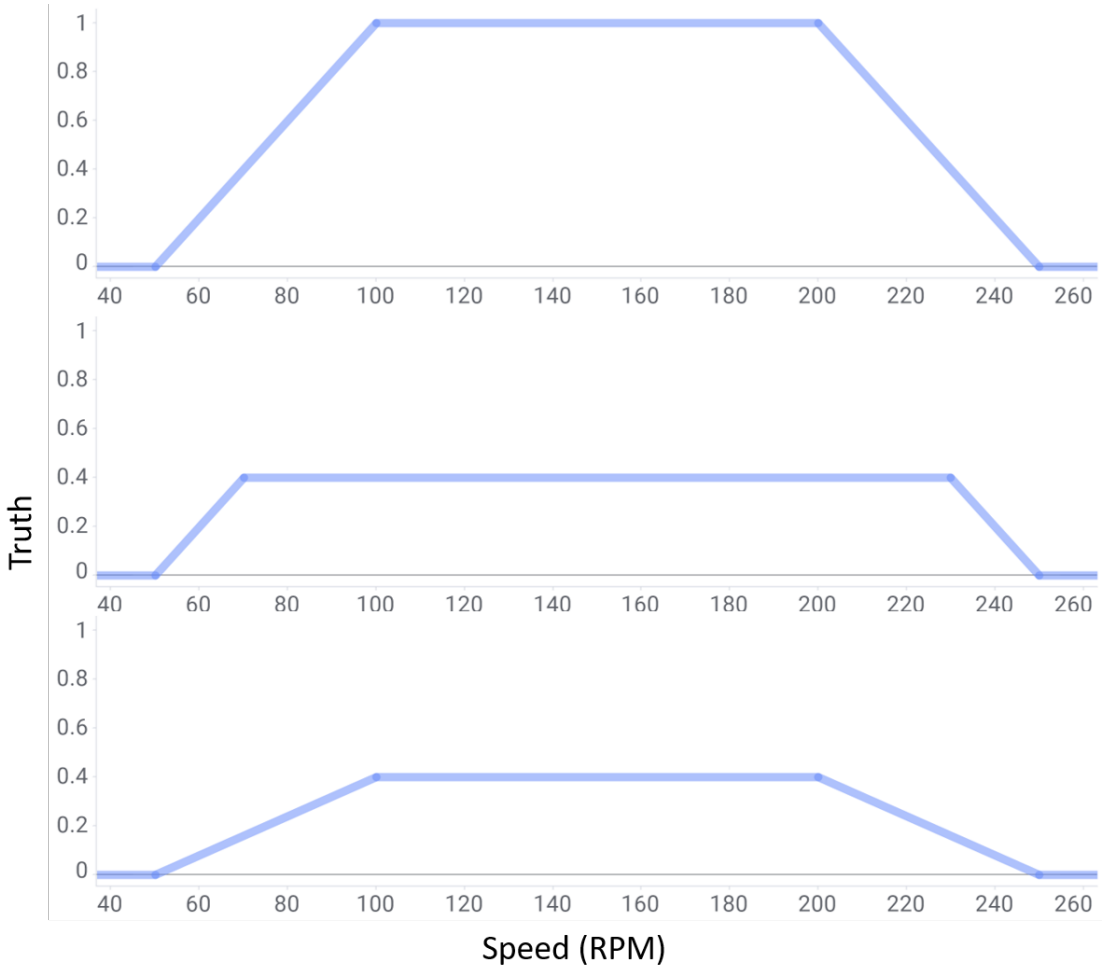

Figure 3.6: Top: base output membership function for the *medium* RPM fuzzy set, determined by rule 2. For 88° F temperature input the antecedent firing strength for this rule is 0.4. Center: The clipped membership function using the minimum implication method. Bottom: The scaled membership function using the product implication method.

5. The next step in the fuzzy inference process is to aggregate the consequent

membership functions for each output. This step combines MFs for each fuzzy sets' rules, then combines the MFs for each outputs' fuzzy sets, resulting in a single, combined, consequent membership function for each system output. Aggregation methods include summing the function sets, taking the maximum of the functions, or averaging the functions. The implicated membership functions for each output set in the running example input of 88°F are shown in Fig. 3.7, assuming a product implication method, and neglecting the schedule input. The aggregation of these membership functions for the fan speed output is shown Fig. 3.8, comparing the sum and max aggregation methods. The output of this process is a single membership function for each output, providing a truth value for every possible output value across the allowed range.

6. The final step in the process is to select a single, most-true crisp output value from the aggregated membership function. This value is deemed representative of the function. The maximum is one seemingly obvious choice, though the use of trapezoidal membership functions can result in the maximum truth value may occurring in multiple places, or as a plateau. To circumvent this, a series of "maxima" defuzzification methods exist, to select the highest or lowest output value corresponding to the maximum truth, or the average of the maxima range. The bisector method selects the output value that divides the area under the output membership function into two equal areas. Similarly, the centroid method selects the output value corresponding to the centroid of the area, that is the line along which the shape would balance if it were a plate of uniform density. Fig. 3.9 compares these defuzzification methods on some example final, aggregated

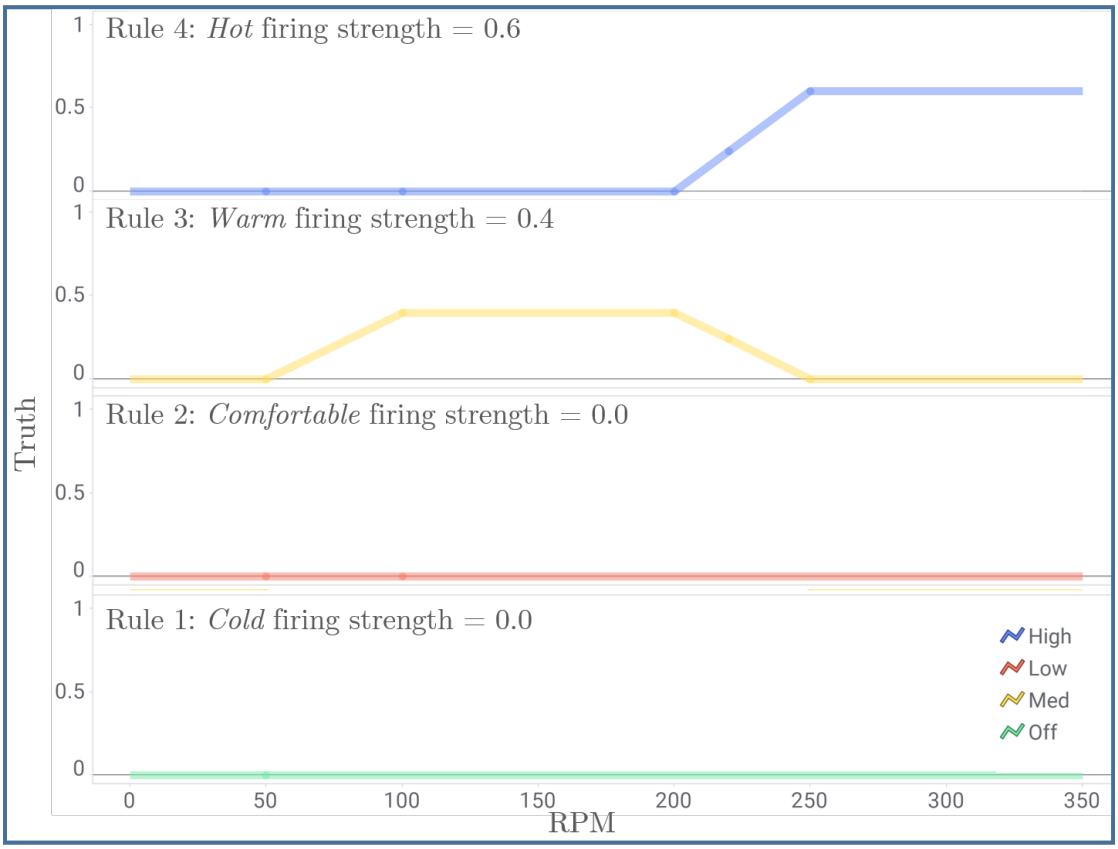

Figure 3.7: Implicated membership functions for each fuzzy set of the RPM output, assuming an input of 88°F and a product implication method. These functions are the input to the aggregation step.

membership functions.

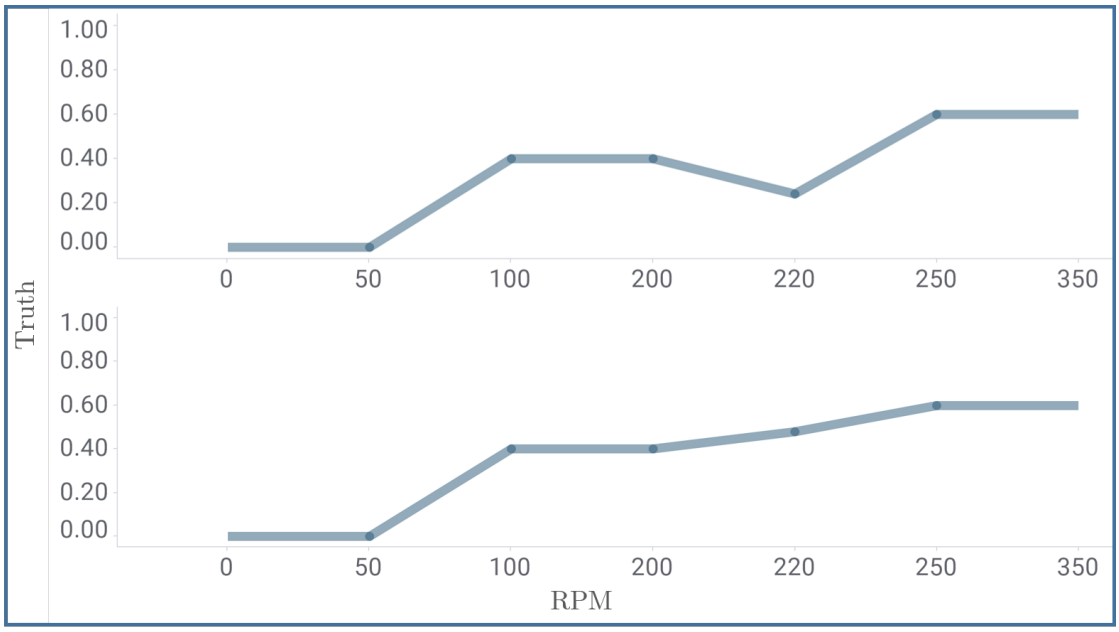

Figure 3.8: Top: Aggregation of the consequent membership functions in Fig. 3.7 using a maximum aggregation method. Bottom: The same aggregation using a sum aggregation method.

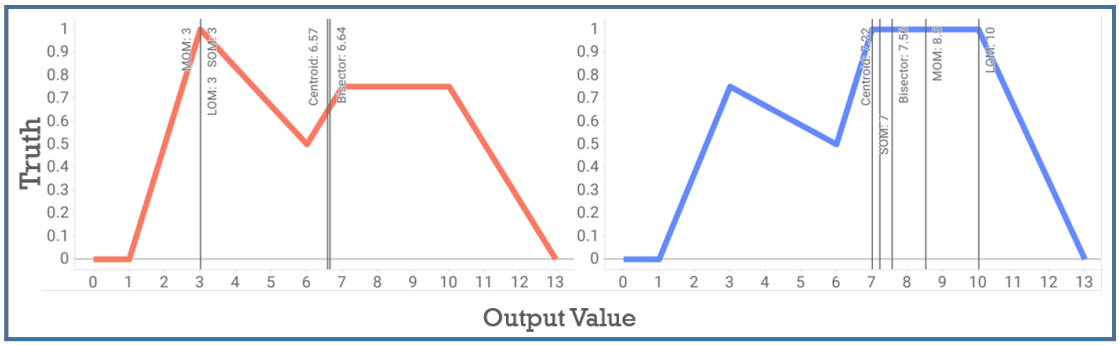

Figure 3.9: Comparison of defuzzification methods on two example output membership functions. It is also of note that if the membership function is symmetric, the bisector and centroid values will be equal.

Chapter 4: Fuzzy Control for Over Travel Protection

In this chapter, a fuzzy control system is implemented for a wave energy converter in WEC-Sim.

4.1 Motivation

In exploring nonlinear control techniques, fuzzy logic control was selected for WEC-Sim as a typical user may not have controls experience or expertise, but may still need to have a nuanced control strategy. While maximizing the power extracted is an obvious priority for a generation device, other concerns exist when designing for marine applications. Considerations for operator and wildlife safety, protection from extreme weather events, minimizing stress, environmental responsibility, shipping lanes and fishing grounds may compete with the objective of extracting energy. Also, when in early development, researchers may want to account for these types of requirements as much as possible, but may be lacking the data or need for precise implementations of the control system. Further, WEC prototyping in the early design cycle may need the control systems to adapt to sudden changes in the WEC body design, or the intended environment. A fuzzy logic controller offers a way to quickly build control systems nuanced enough to handle competing, possibly nonlinear objectives, but flexible enough to handle changes during early

development.

In order to incorporate fuzzy control into WEC-Sim, an in-application example for a WEC was created which could be adapted as needed to other applications. The objective of the fuzzy logic controller was to limit the movement of the float of the RM3 model within an expected nominal range in addition to an optimal passive linear damping strategy if the float was within the nominal range. The theory for this control assumes that a rated range of motion exists for the device, and during out-of-specification wave conditions, the PTO drive could be operated to shed power in order to maintain operation within the limits. This power shedding operation would be preferable to having to come offline completely to avoid out of specification operation. This example is analogous to a wind turbine pitching its blades in high wind speeds, shedding power in order to slow rotation to within the limits of the generator. A block diagram for this WEC control system is shown in Fig. 4.1.

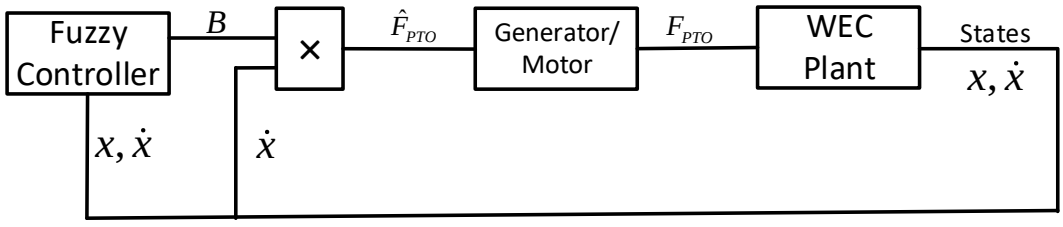

Figure 4.1: A block diagram for the system. Using the position and velocity states of the WEC, the Fuzzy Controller supplies a damping value which is used to calculate the motor's commanded PTO force.

4.2 Methods

Fig. 4.2 and 4.3 show the input membership functions used for position and velocity, respectively. The operating range for these inputs are selected based on the performance of the linearly damped point absorber under nominal wave conditions, which were assumed as a 2 meter wave height and a period of 8 seconds. The relative velocity of the float is considered "too fast" when it reaches the maximum speed achieved at the expected wave conditions, as such both membership functions, the positive and negative directions, become fully true at this time. The position membership functions include the "middle," considered anywhere in the expected operating range, and upper and lower over-travel limits, which become fully true at the edges of the nominal range. When the float begins to travel outside the nominal range, the controller should respond by over-damping the float, increasing mechanical impedance, to keep it within the limits. The following rules will achieve this

1. If position is middle, then PTO force is linearly damped
2. If position is too high and velocity is too fast up, then PTO force is over-damped
3. If position is too low and velocity is too fast down, then PTO force is over-damped

The damping value provided by the controller will either be the predetermined optimal passive-damping value[1], for the nominal wave conditions (overdamping multiplier = 1) or an increasingly over-damped value as the float travels out of the

[1] derived in section 2.1

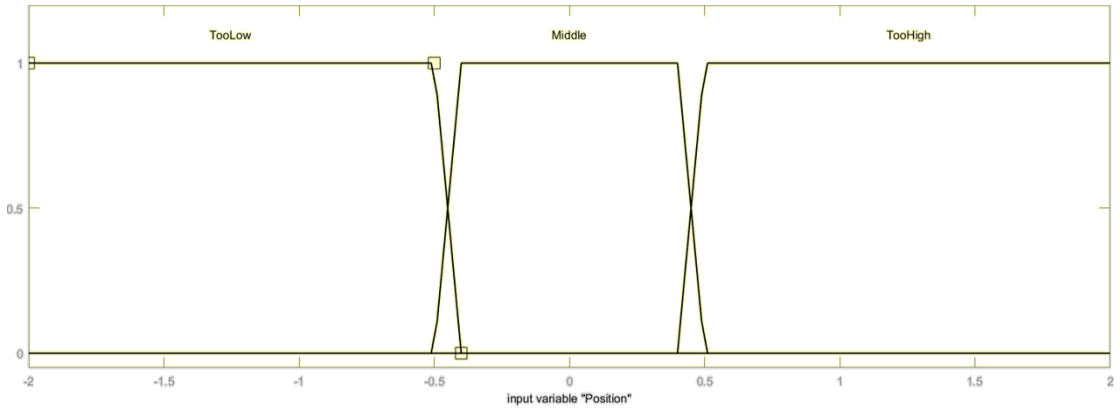

Figure 4.2: The Membership Functions for relative position of the float and spar.

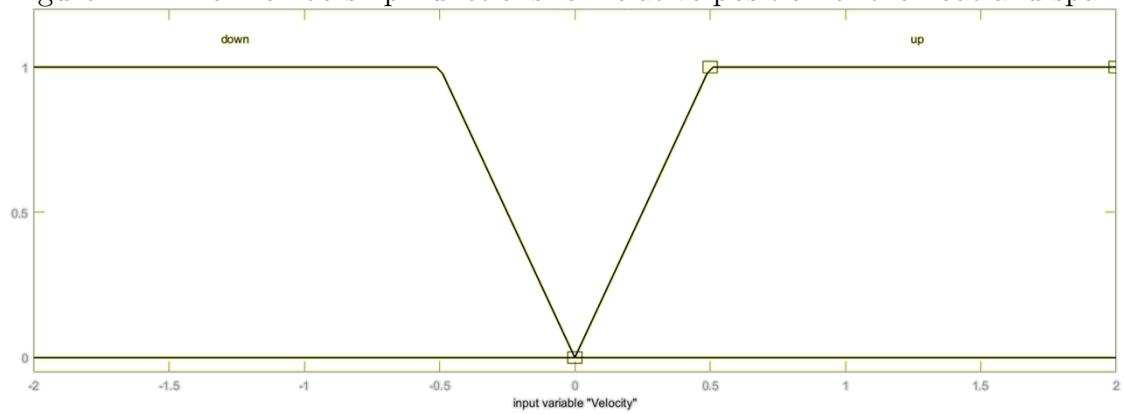

Figure 4.3: The Membership Functions for relative velocity of the float and spar.

allowed range, and the overdamping multiplier increases. An assumption of the simulation is that the PTO can act upon the bodies anywhere along their range of motion. For example, if the PTO is achieved via a linear generator, the model assumes there are sufficient coils along the RM3's spar to affect the float anywhere waves might take it, and it will never be out of reach of the generator. This model was simulated under several conditions to evaluate the effectiveness of the fuzzy controller.

This fuzzy logic controller was implemented using MATLAB's Fuzzy Logic Toolbox for Simulink, however to prevent requiring additional expensive MATLAB licensing, a custom fuzzy library of functions was created and the system was implemented using this as well. The custom functions allow for an arbitrary number of inputs, membership functions, rules and outputs, and have clear instructions along with the example for the function expectations. Many of the operations and methods available in the Fuzzy Logic Toolbox were implemented, and any additional options desired could be implemented on top of the existing framework. A further description of the custom fuzzy logic script can be found in Appendix A.

4.3 Results

Six initial simulations in Simulink were run for comparison, basic linear damping without over-travel protection was compared with the fuzzy controller for at the nominal and high sea states, using the Fuzzy Logic Toolbox and the custom fuzzy function script. Each simulation used the 'regular' wave class in WEC-Sim for a total simulation time of 500 seconds with 100 seconds of wave ramp time. This wave class assumes steady state waves with constant added mass and radiation damping coefficients to avoid performing the convolution integral. The reactive portion of PTO impedance was also assumed to be 0. The left plot of Fig. 4.4 shows the float's relative position under the nominal, two meter waves sea state using the custom fuzzy script. The linearly damped model (blue, covered) is plotted with the model including the fuzzy control (orange). The result of the over-damping

for position control is a compromise of 7.31% of the captured energy over the 500 seconds of the simulation. It may be possible to decrease the losses incurred while in the nominal range through tuning, with the trade-off of subjecting the PTO to more sudden forces. A similar plot is shown for a wave height of three meters on the right of Fig. 4.4. This plot shows that the fuzzy logic controller is capable of limiting the motion of the float in high wave heights, while maintaining comparable power performance to a linearly damped PTO when waves are in the nominal operating range. This figure was also generated using the custom fuzzy logic script as opposed to the toolbox. For comparison, the position using the toolbox to implement the identical control system for regular waves is shown in Fig. 4.5. The two systems perform similarly in limiting the relative position of the float and spar for the early simulation, however for longer simulation times the system implemented using MATLAB's Fuzzy Logic Toolbox displays a ringing effect on the position. This can be tuned out by increasing the sensitivity of the output damping-multiplier, and is likely due to differences in the implementation of limits for the system inputs, and default output values when no rule fires. An irregular wave simulation using a Bretschnieder wave spectrum with identical waveheight and period conditions is shown in Fig. 4.6.

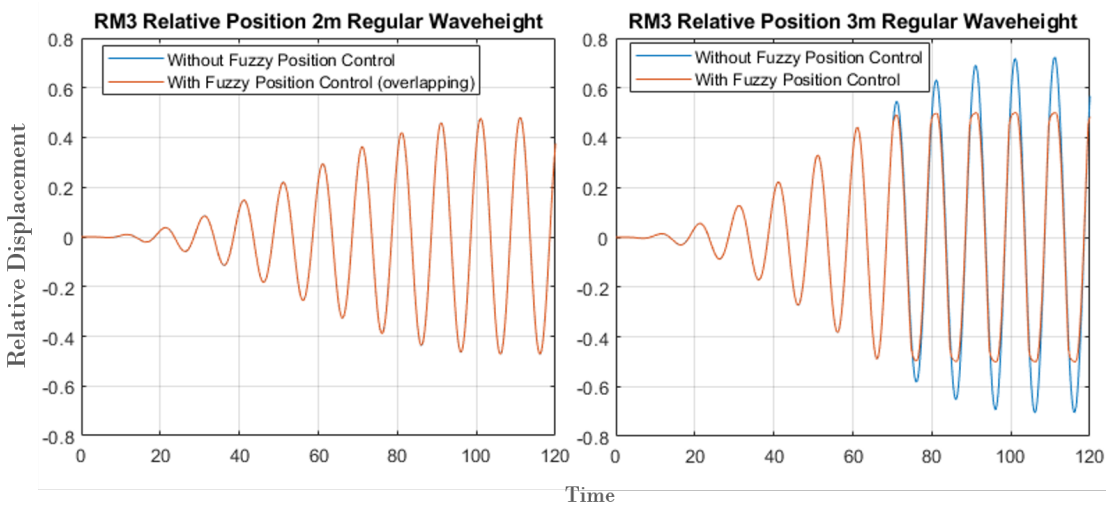

Figure 4.4: Relative position of spar and float of RM3 in the selected nominal (left) and high (right) sea states. Passively damped control is compared with fuzzy over travel protection.

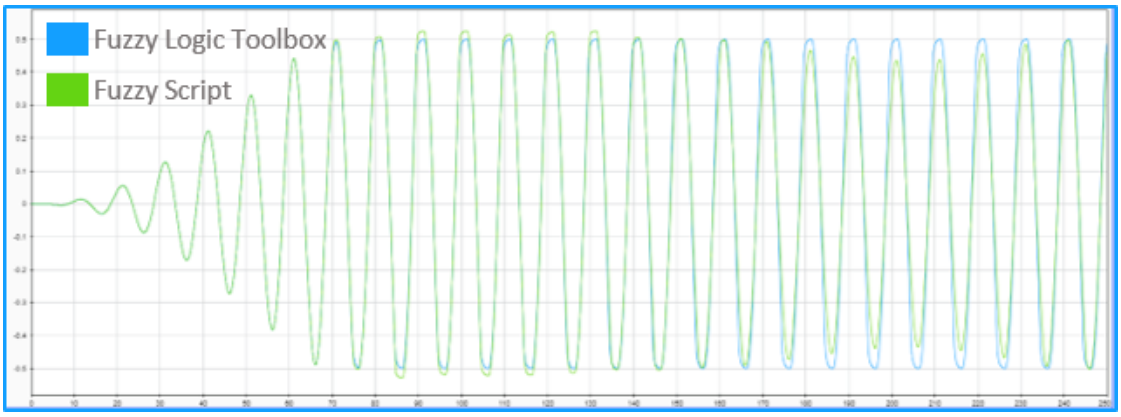

Figure 4.5: Comparison of over-travel protection position limiting using the Fuzzy Logic Toolbox vs the custom fuzzy script under the identical simulation conditions.

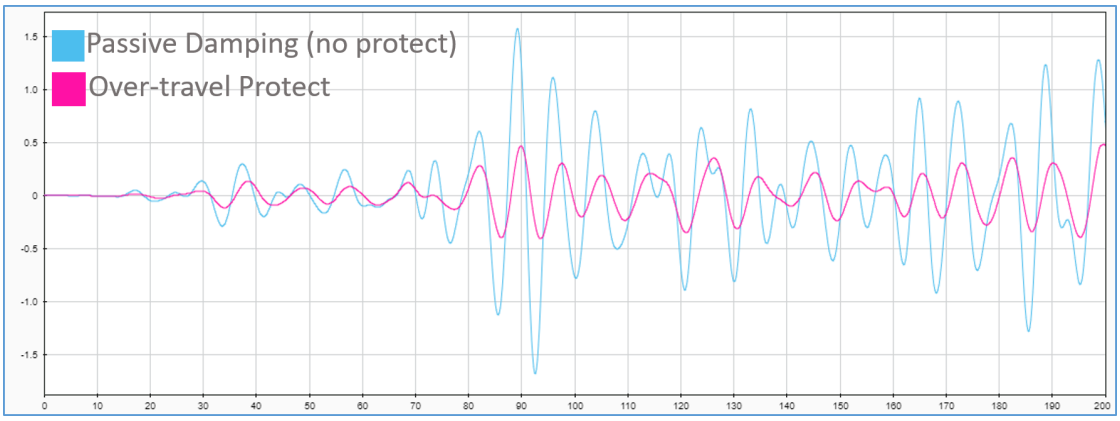

Figure 4.6: Relative position of spar and float of RM3 in the high sea states with irreguar wave spectra. Passively damped control (blue) is compared with fuzzy over travel protection (magenta.)

Chapter 5: A 2-level Nonlinear WEC Control Scheme

In order to create a system which could respond optimally to real-time wave conditions, the fuzzy logic controller described in Chapter 4 was modified. Since period was determined to be the biggest factor in setting the control parameters for the reactive control strategies described in Section 2.2, an additional input was added to the system for the average wave period. The resulting system is shown in Fig. 5.1, with the added function of setting optimal PTO damping and stiffness using fuzzy logic. This input was estimated by taking a 10 second rolling sample window of waveheight and using a Fast Fourier Transform to determine the primary frequency and thus period. The period was used in a set of rules dictating B_{pto} and C_{pto}. The fuzzy sets and membership functions for this input period were determined based on the quartiles of measurements from the National Data Bouy Center, using Station 46050, Stonewall Bank, 20NM West of Newport, OR for the year of 2018. The period and waveheight for the samples are shown in Fig. 5.2, with the values used for the edges of the fuzzy sets indicated.

The input and output membership functions are shown in Fig. 5.3, and the additional rules for the system are:

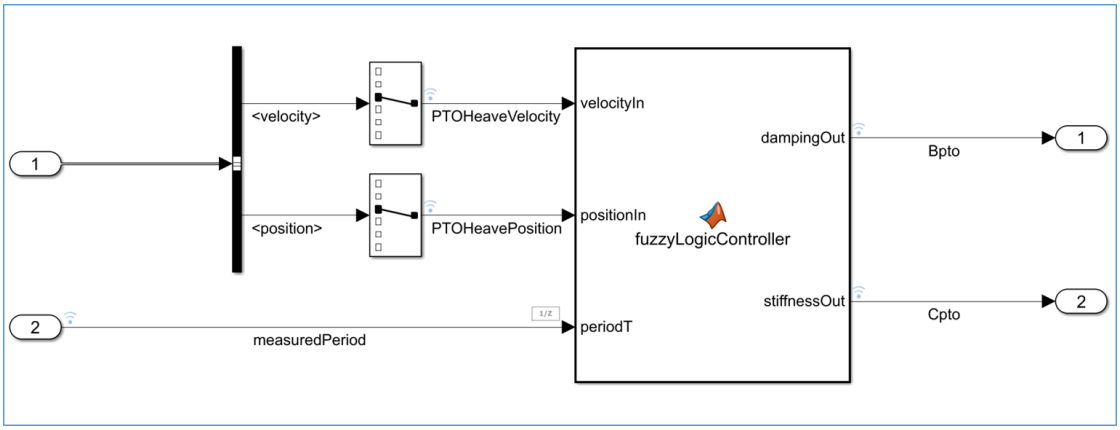

Figure 5.1: Supervisory level for the 2 level system, using fuzzy logic to set optimal values for Bpto and Cpto and enforcing over-travel protection.

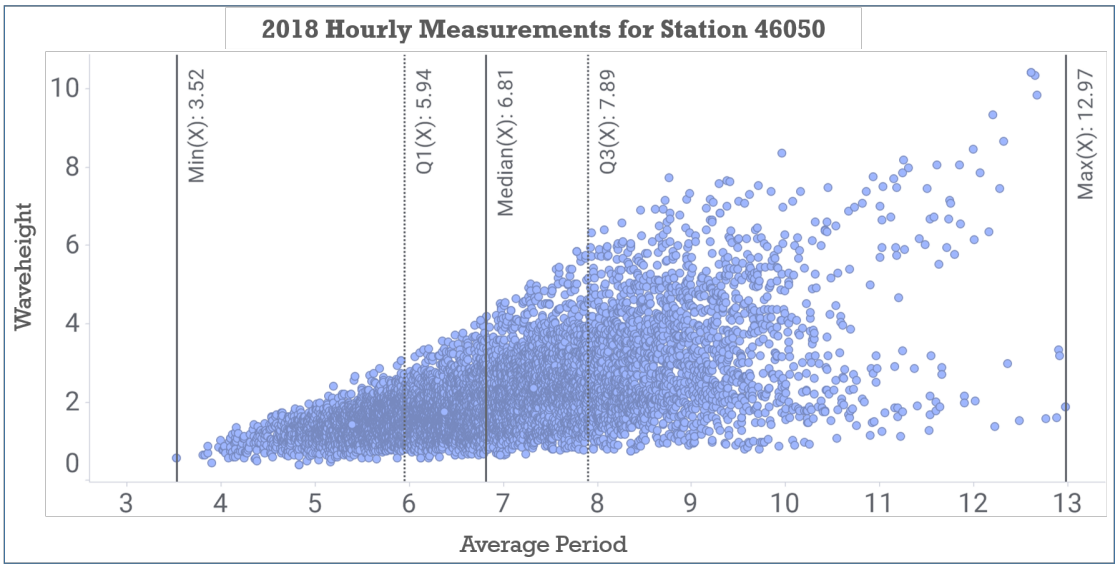

Figure 5.2: Hourly samples for average period and waveheight in 2018 at the Stonewall Bank bouy.

1. If period is *min*, damping is *min Damping*
2. If period is *q1*, damping is *q1 Damping*
3. If period is *median*, damping is *median damping*
4. If period is *q3*, damping is *q3 Damping*
5. If period is *max*, damping is *max Damping*
6. If period is *min*, C_{pto} is *min-Pd* C_{pto} *value*
7. If period is *q1* or med or q3, Cpto is C_{pto} *limit*
8. If period is *max*, C_{pto} is *max-Pd* C_{pto} *value*

The output membership functions are shown in Fig. 5.4 and 5.5. Note that these membership functions are impulse type. The implication method is the product, multiplying the impulse value by the rule firing strength, and the aggregation type is summation. The input MFs are organized such that the implication and aggregation methods achieve defuzzification via a weighted average of the fired impulse functions. The result of this system is a sort of interpolation between set lookup values which were calculated based on representing the wave sample space. While some of the readability and linguistic intuition is lost, Fig. 5.6 compares the accuracy of the fuzzy system to the complete process of calculating the optimum parameters based on interpolation of the hydrodynamic parameters produced by the BEM solver. It is clear in Fig. 5.6 that the Fuzzy system accurately selects B_{pto} and C_{pto} for the most common operating regions present in the bouy period data, while not performing as well at the more extreme periods.

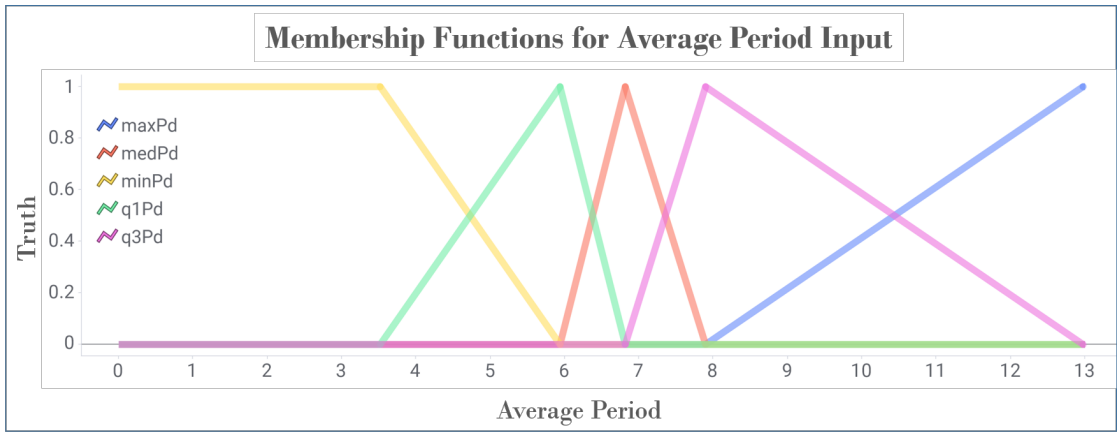

Figure 5.3: Membership functions for average period input, based on quartile values in Fig. 5.2 from one year worth of hourly sample data.

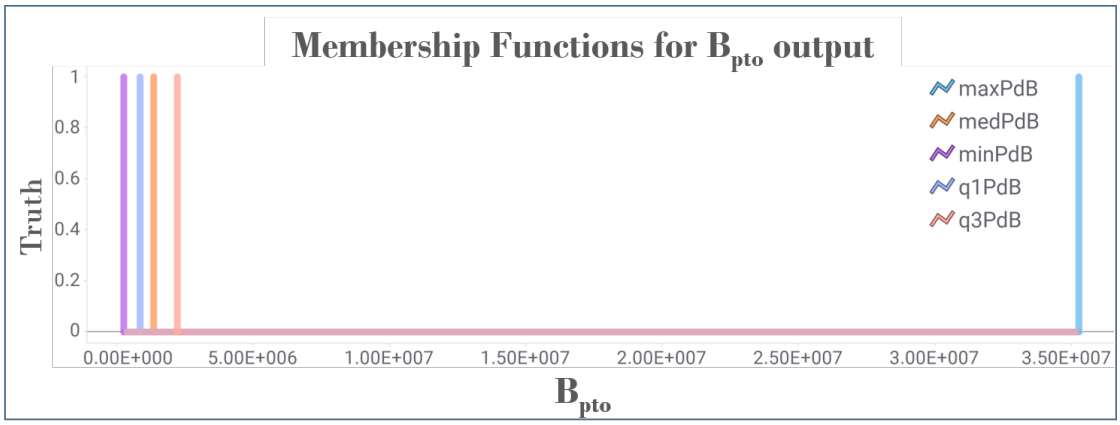

Figure 5.4: Impulse membership functions for B_{pto} as calculated according to the intrinsic impedance in appendix B and optimal B_{pto} determined by equation 2.11 for the given period.

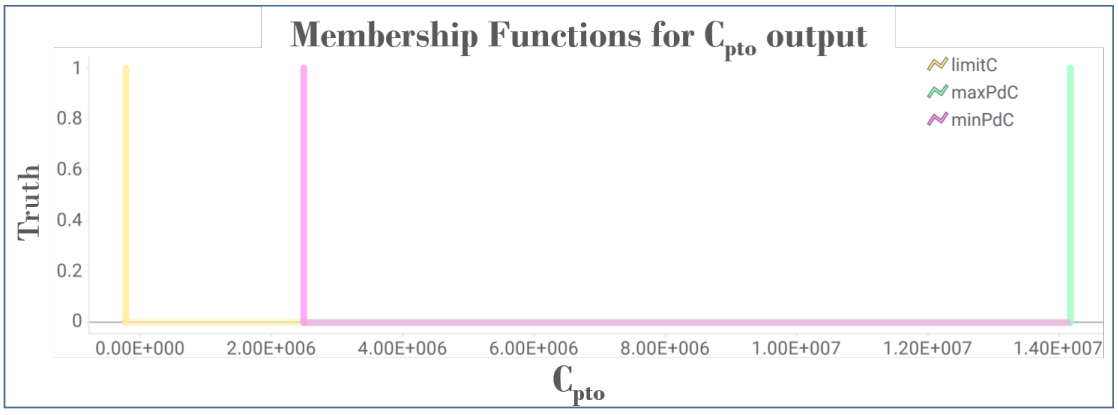

Figure 5.5: Impulse membership functions for C_{pto} as calculated according to the intrinsic impedance in appendix B and optimal C_{pto} determined by equation 2.12 for the given period.

5.1 Results

The plot of the spar and float's relative positions is shown in Fig. 5.7, using a Bretschnieder irregular wave spectrum with a 9s primary period. The top left

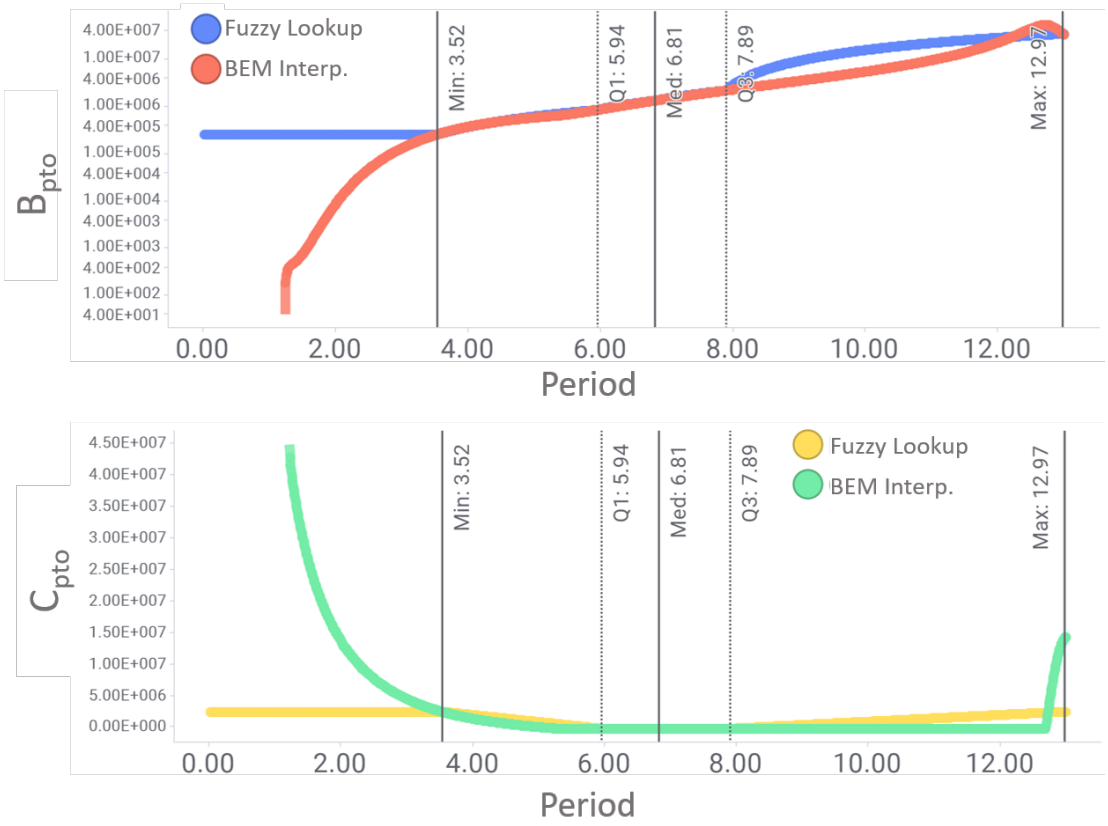

Figure 5.6: Comparison of the optimal B_{pto} and C_{pto} control values determined by the fuzzy interpolation controller vs. using the hydrodynamic properties and linear interpolation.

plots show the wave elevation, which were seeded identically so the only difference is the primary elevation. In the higher wave condition the system limits the motion of the WEC while still using the optimal control values for power take-off, based on the real time period estimation.

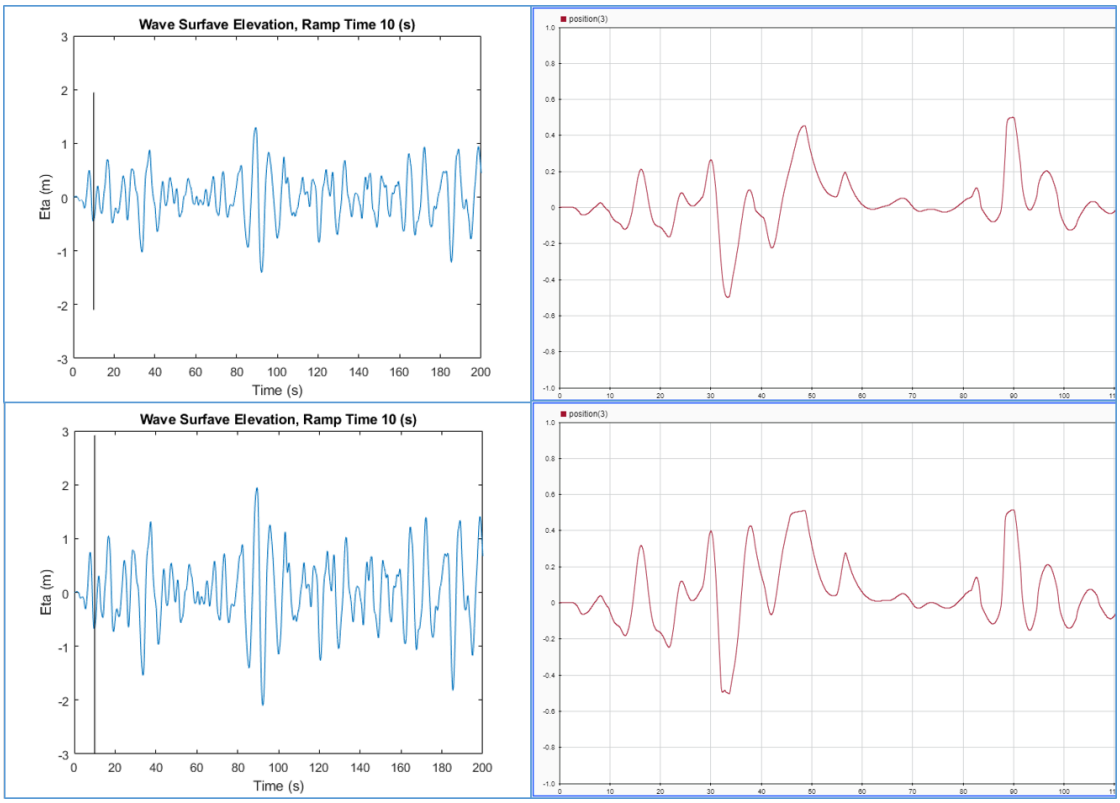

Figure 5.7: Comparison of the combined fuzzy over-travel protection and optimal reactive control script under nominal wave conditions (top) and high wave conditions (bottom) using a Bretschneider irregular wave spectrum (left).

Chapter 6: Conclusion

While a fuzzy system which approximates the nonlinear control law might have captured more power, the lack of understanding of the behavior of this law prevented complete implementation. In order to accurately apply the law for optimal power take-off, fmincon would need to be used to optimize the parameters as the sea state changed. Since the computation time for fmincon to arrive at the optimal parameters was too high, real time tracking of the period to set the nonlinear control law is not practical until the law is better understood, or computation time can be significantly reduced. As stated in section 1.1, finding the exact mechanism by which the nonlinear control law is able to perform better than the linear strategies was not deemed in scope for this work. Whereas the pursued exploration of applying nonlinear fuzzy logic controls to a wave energy converter in WEC-Sim was accomplished. A pull request was created to add the fuzzy over-travel protection script and Fuzzy Logic Toolbox implementations to the WEC-Sim_Applications repository. Possible future improvements to this contribution include changing the implementation of the fuzzy script to define a separate class for membership functions and rules. This is closer to how the Fuzzy Logic Toolbox is implemented, and leaves less room for error when designing systems, though may be partially responsible for the slightly longer computation time when using the toolbox. Similarly, some of the design decisions for the controller may be better suited to exist in the

wecSimInputFile.m which is run prior to for every simulation. This change would consolidate where modifications to the simulation are done, and prevent the fuzzy system's design parameters from being redefined every time step of the simulation.

Other future improvements include expanding the nonlinear control strategies employed, adding examples to WEC-Sim_Applications implementing control strategies using nueral networks, or reinforcement learning, as other researchers have already demonstrated for WEC simulations outside of WEC-Sim.

The model discussed in Chapter 5 may also be helpful to provide as a nonlinear control example, however, as shown in Fig. 5.6, using a script which directly calculates the optimal B_{pto} and C_{pto} provides better accuracy without a loss in computation time, and the use of fuzzy logic to interpolate between predetermined lookup values may not be the best instructive example for those unfamiliar with fuzzy logic.

Presented is an application of nonlinear control strategies to a heaving point absorber wave energy converters in WEC-Sim, as a contribution the WEC-Sim community. A generally nonlinear control law was extended from the established reactive linear control strategy. Several methods were used to experimentally optimize the nonlinear law, eventually determining that it was capable of producing more power than the linear reactive control strategy. A simple fuzzy logic controller was used to add a competing objective to a typical passive damping control strategy for optimizing power. This controller was implemented using the off-the shelf Fuzzy Logic Toolbox, as well as in a custom script not requiring additional licensing. A real time period tracking model was created, using a fuzzy controller

to set the optimal parameters for the reactive damping control strategy, and this framework could be valuable if extended to the generally nonlinear control law, once that law can be better described. The findings of these experiments were packaged as a set of tutorials in the WEC-Sim_Applications repository, so that they might be beneficial to the research community, and support the adoption of WEC technology to meet electricity needs.

Bibliography

[1] P. Jacobson, "Mapping and Assessment of the United States Ocean Wave Energy Resource," Electric Power Research Institute, Tech. Rep., 01 2010.

[2] J. Andrews and N. Jelley, *Energy Science Principles, Technologies, and Impacts*, 3rd ed. Oxford University Press, 6 2017.

[3] K. Ruehl, C. Michelen, S. Kanner, M. Lawson, and Y.-H. Yu, "Preliminary verification and validation of wec-sim, an open-source wave energy converter design tool," ser. International Conference on Offshore Mechanics and Arctic Engineering, vol. Volume 9B: Ocean Renewable Energy, 10 2014. [Online]. Available: https://doi.org/10.1115/OMAE2014-24312

[4] J. Weber, "Wec technology readiness and performance matrix finding the best research technology development trajectory," ser. International Conference on Ocean Energy. National Hydropower Association, 10 2012, an optional note.

[5] Y.-H. Yu, M. Lawson, K. Ruehl, and C. Micheln Strfer, "Development and demonstration of the wec-sim wave energy converter simulation tool," ser. 2nd Marine Energy Technology Symposium, 01 2014.

[6] "Wec-sim overview," http://wec-sim.github.io/WEC-Sim/overview.html, date Accessed: 2019-08-23.

[7] D. Valrio, M. J. Mendes, P. Beiro, and J. S. da Costa, "Identification and control of the aws using neural network models," *Applied Ocean Research*, vol. 30, no. 3, pp. 178 – 188, 2008. [Online]. Available: http://www.sciencedirect.com/science/article/pii/S0141118708000679

[8] E. Anderlini, D. Forehand, E. Bannon, and M. Abusara, "Reactive control of a wave energy converter using artificial neural networks," *International Journal of Marine Energy*, vol. 19, pp. 207 – 220, 2017. [Online]. Available: http://www.sciencedirect.com/science/article/pii/S2214166917300668

[9] E. Anderlini, D. Forehand, E. Bannon, Q. Xiao, and M. Abusara, "Reactive control of a two-body point absorber using reinforcement learning,"

Ocean Engineering, vol. 148, pp. 650 – 658, 2018. [Online]. Available: http://www.sciencedirect.com/science/article/pii/S0029801817304699

[10] M. Jama, A. Wahyudie, A. Assi, and H. Noura, "An intelligent fuzzy logic controller for maximum power capture of point absorbers," *Energies*, vol. 7, 06 2014.

[11] L. Wang and J. Isberg, "Nonlinear passive control of a wave energy converter subject to constraints in irregular waves," *Energies*, vol. 8, p. 6528, 07 2015.

[12] D. Son and R. W. Yeung, "Real-time implementation and validation of optimal damping control for a permanent-magnet linear generator in wave energy extraction," *Applied Energy*, vol. 208, pp. 571 – 579, 2017. [Online]. Available: http://www.sciencedirect.com/science/article/pii/S0306261917313806

[13] J. Falnes, *Ocean Waves and Oscillating Systems: Linear Interactions Including Wave-Energy Extraction*. Cambridge University Press, 2002.

[14] ——, "Optimum control of oscillation of wave-energy converters," *International Journal of Offshore and Polar Engineering*, vol. 12, 06 2002.

[15] J. Todalshaug, J. Falnes, and T. Moan, "A comparison of selected strategies for adaptive control of wave energy converters," *Journal of Offshore Mechanics and Arctic Engineering*, vol. 133, 03 2011.

[16] J. Todalshaug, T. Bjarte-Larsson, and J. Falnes, "Optimum reactive control and control by latching of a wave-absorbing semisubmerged heaving sphere," vol. 4, 01 2002, pp. 415–423.

[17] R. H. Byrd, M. E. Hribar, and J. Nocedal, "An interior point algorithm for large-scale nonlinear programming," *SIAM J. on Optimization*, vol. 9, no. 4, pp. 877–900, Apr. 1999. [Online]. Available: http://dx.doi.org/10.1137/S1052623497325107

[18] R. H. Byrd, J. C. Gilbert, and J. Nocedal, "A trust region method based on interior point techniques for nonlinear programming," *Mathematical Programming*, vol. 89, no. 1, pp. 149–185, Nov 2000. [Online]. Available: https://doi.org/10.1007/PL00011391

[19] R. Waltz, J. Morales, J. Nocedal, and D. Orban, "An interior algorithm for nonlinear optimization that combines line search and trust region steps,"

Mathematical Programming, vol. 107, no. 3, pp. 391–408, Jul 2006. [Online]. Available: https://doi.org/10.1007/s10107-004-0560-5

APPENDICES

Appendix A: Custom Fuzzy Logic Function Library

This section provides a description of the functions and main script expectations of the custom fuzzy logic script. Since the fuzzy code was implemented with the Simulink "MATLAB Function" block, all design decisions had to support code generation. In particular, great care had to be taken to preallocate all variables, which presented a significant design challenge for writing functions that could be used to support fuzzy systems with an arbitrary number of system inputs and outputs. The script is generally organized with a main script following the fuzzy inference process as outlined in Chapter 3, with functions defined for each step in the process. Fuzzy sets' membership functions are organized into structures with fields defining their types and the important values, which are then substructed under the relevant inputs. Similarly, rules and their antecedants, output membership functions, aggregation methods and consequent membership functions are organized into structures. This organization is expected by the functions used to evaluate the system. A complete figure of the flow of the function calls of the main script is shown in Fig. A.1, and the following section is an index of the functions and their requirements.

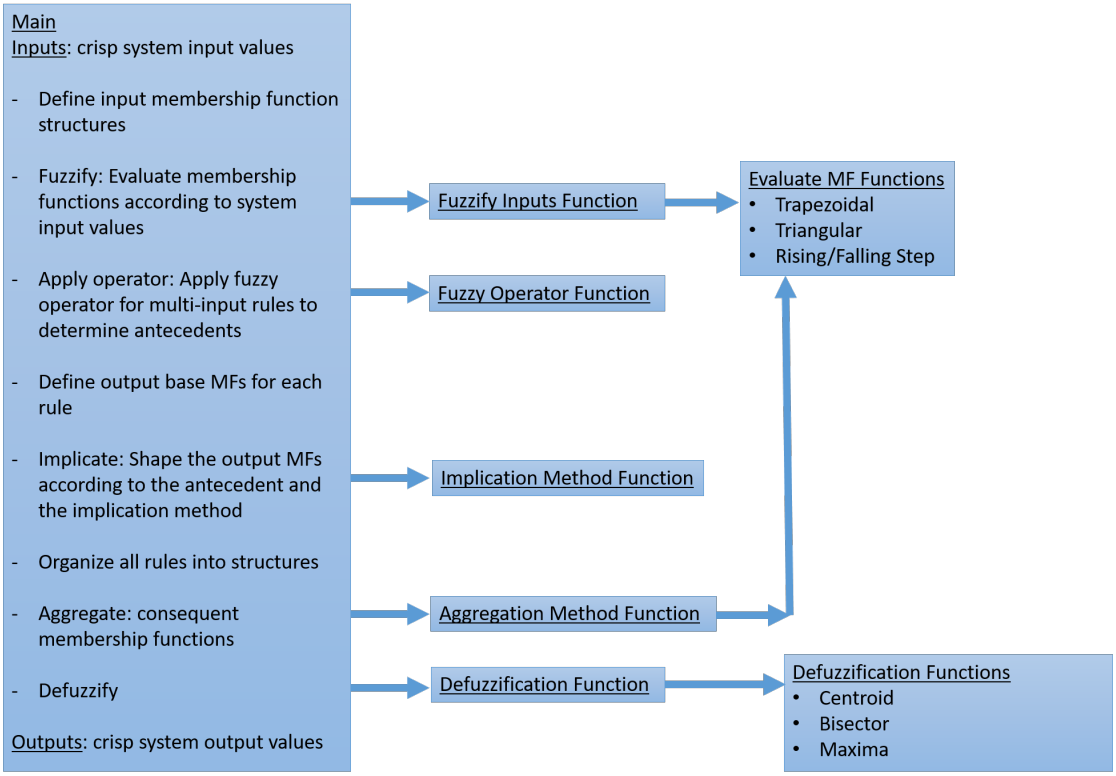

Figure A.1: Flowchart of function calls for the custom fuzzy script.

A.1 Fuzzy Script Function Index

A.1.1 fuzzifyInputs

The fuzzifyInputs function takes the system input values and evaluates the relevant membership functions to return the truth value for each function. Calls any of a number of evaluation functions based on membership function type.

Inputs:

1. inValue: a crisp system input value

2. MFs: struct of fuzzy set membership functions for an input. supported values for MFs.type: ‘triangle’,‘step’,‘down step’,‘trap’

Outputs:

1. fuzzifiedInput: the same struct MFs, with the percentTrue field set according to the crisp input and memberhsip function

A.1.2 applyFuzzyOperator

This function applies a fuzzy operator to produce a single antecedent value for multi-input fuzzy rules.

Inputs:

1. inputMembershipTruth: vector of analog truth values for input membership function values relevant to rule

2. : fuzzyOperator: supported values: ‘minAnd’, ‘prodAnd’, ‘sumOr’, ‘maxOr’, ‘average’

Outputs:

1. antecedentTruth: the same struct MFs, with the percentTrue field set according to the crisp input and memberhsip function

A.1.3 applyImplicationMethod

This function implicates a fuzzy rule according to the specified implication method.

Inputs:

1. antecedent: single truth value for the rule's antecedent
2. outputMembership: membership function structure for output
3. implicationMethod: an implication method, supported values {'prod', 'min'}

Outputs:

1. consequentMF: system output membership function shaped by the antecedent

A.1.4 evalMF

General function to evaluate membership functions, which may have a max value less than 1. This function calls from a set of supporting functions based on the MF.type field.

Inputs:

1. inValue - value to evaluate membership for
2. MF: membership function struct which expects a 'maxVal' field. Supported values for MF.type: {'triangle','step','down step','trap'}

Outputs:

1. Single analog truth value

A.1.5 performAgg

Function to aggregate consequent membership function's for fuzzy sets' relevant rules, and outputs' relevant fuzzy sets. **Inputs:**

1. truthMatrix: matrix where each row represents the truth value of the corresponding rule's membership function, evaluated at the necessary points to get a complete detailed aggregation

2. aggregationMethod: Supported values for aggregationMethod: {'max','min', 'mean','prod','sum'}

Outputs:

1. singleTruthFunction: a row matrix aggregated according to the aggregationMethod, along the row dimension

A.1.6 defuzzify

A function to defuzzify the final membership functions and set the fuzzy controller's outputs. A call to this function is not required in the output membership functions are the impulse type. **Inputs:**

1. outputFun : struct for a system output with a field containing the 2-row vector of the aggregated membership functions, and a range field

2. defuzzificationMethod : Supported values for aggregationMethod: {'centroid','bisector','LO

Outputs:

1. crisp: crisp value for system output

Appendix B: Mechanical Impedance Analogy to Electrical Domain

The mechanical impedance analogy is one of several analogies which exploit the fact that the differential equations describing many natural phenomenon are of the same form. In particular, the mechanical impedance analogy applies the concepts and representation of electrical systems via the complex generalization of Ohm's law, to analogous mechanical systems, using the concept of mechanical impedance, a term relating harmonic forces with velocities acting on the mechanical system:

$$F(\omega) = Z(\omega) \cdot u(\omega)$$

Where,

- $F(\omega)$ is force, analogous to voltage
- $u(\omega)$ is velocity, analogous to current
- $Z(\omega)$ is mechanical impedance, analogous to electrical impedance

In this relation, $Z(\omega)$ is composed of mechanical resistance R_m and mechanical reactance X_m, such that

$$Z(\omega) = R_m(\omega) + jX_m(\omega)$$

Where the analogous R_m refers to damping within mechanical systems. Mechanical reactance can be used to extend the analogy further to inductance and capacitance. Voltage in an inductor is written $v = L\frac{di}{dt}$, which when the analogy is applied, gives the relation for Newton's Second law of motion

$$F = m\frac{du}{dt}$$

Thus the mass, m can be treated as inductance, with mechanical impedance $Z_m = j\omega m$. For the mechanical analog of capacitance, *compliance*, the inverse of stiffness gives the direct analogy, but it is important to note that the convention used in this work is to relate stiffness, for which C is used. Thus, the relation for stiffness is written

$$Z_m = \frac{C}{j\omega} = -j\frac{C}{\omega}$$

Finally, an advantage for our case, is the conversion between electrical and mechanical power, the goal of our wave energy converter.

$$P = Fu$$

When applied to the heaving point wave energy converter, consisting of the float, spar, and linear generator PTO between them, we can represent the system with the circuit in Fig. B.1.

Where

· F_{pto} is force applied by the PTO generator

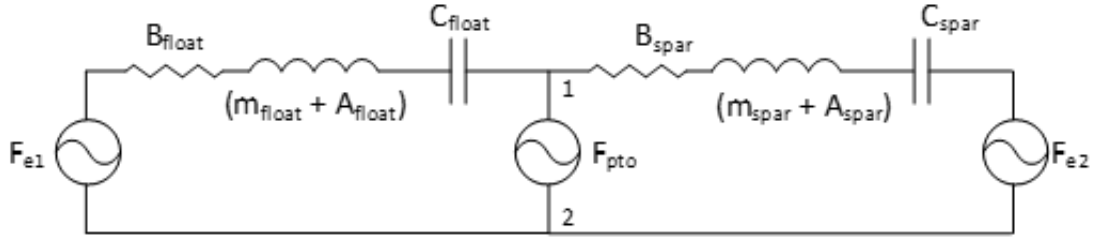

Figure B.1: Mechanical circuit for 2-body point absorber with a PTO between the bodies, using the mechanical impedance analogy.

- F_e is the wave excitation force on each respective body
- m is the respective body's mass
- A is the respective body's added mass
- B is the respective body's damping
- C is the respective body's stiffness

For the purpose of defining a control law, we would like to derive an expression for the impedance "seen" at the terminals of the PTO generator, terminals 1 and 2. Applying Thévenin's Theorem, F_{pto} is removed, F_{e1} and F_{e2} are shorted, and the Thévenin Impedance seen across terminals 1 and 2 is $Z_i = Z_{float}||Z_{spar}$, where

$$Z_{float} = B_{float} + j(\omega(m_{float} + A_{float}) - \frac{C}{\omega})$$
$$Z_{spar} = B_{spar} + j(\omega(m_{spar} + A_{spar}) - \frac{C}{\omega})$$

It is this expression which is meant by the intrinsic impedance of a heaving point absorber, used in derivations for the control laws Described in Section 2.1 and Section 2.2. The values for added mass, radiation damping and linear restoring stiffness for a range of excitation frequencies are provided by the BEMIO process prior to running WEC-Sim. These values are used to calculate the intrinsic impedance, Z_i, directly leading to the control values of B_{pto} and C_{pto}.

Appendix C: Limit for PTO Counter-Restoring Force

Focusing on the reactive portion of the control impedance, C_{pto}, a stability constraint becomes clear. The restoring force of the point absorber has been defined

$$F_h = -Cz \tag{C.1}$$

and is defined by convention so that it is opposed to the excitation force F_e. A positive excitation force, produces a positive change in the relative position z: the float moves up in relation to the spar, and proportional to how much it moves up, a restoring force is applied to return it to the stable origin position. However, the PTO force, F_{pto} is defined in phase with the excitation force, meaning a positive excitation force, produces a positive change in relative position, which in turn creates a component of the PTO force proportional to and *in the same direction* as the displacement. If this component is not overwhelmed by the other forces present, a positive feedback will create runaway force on the float. To determine the limit for C_{pto} at which this occurs, let $F_{pto} = C_{pto}(z_1 - z_2)$, be defined by the relative position of the bodies. Then, using Newton's second law, the sum of forces

on the float (body 1) and spar (body 2) can be expressed

$$m_1\ddot{z_1} = -B_1\dot{z_1} + C_1 z_1 + C_{pto}(z_1 - z_2)$$
$$m_2\ddot{z_2} = -B_2\dot{z_2} + C_2 z_2 + C_{pto}(z_1 - z_2)$$

Since they do not affect the stability we are interested in, to simplify we can assume $\ddot{z_1} = \ddot{z_2} = 0$ and $B_1 = B_2 = 1$.

$$\dot{z_1} = C_1 z_1 + C_{pto}(z_1 - z_2) \tag{C.2}$$
$$\dot{z_2} = C_2 z_2 + C_{pto}(z_1 - z_2) \tag{C.3}$$

Now assuming the velocity of the spar is relatively small compared to the float, let $\dot{z_2} = 0$, then (C.3) can be rewritten

$$z_2 = \frac{z_1 C_{pto}}{C_2 + C_{pto}} \tag{C.4}$$

and substituting (C.4) into (C.2)

$$\dot{z_1} = z_1(C_1 + C_{pto} - \frac{C_{pto}^2}{C_2 + C_{pto}})$$

This expresses the unstable condition when $(C_1 + C_{pto} - \frac{C_{pto}^2}{C_2 + C_{pto}}) > 0$, or when

$$C_{pto} > \frac{-C_1 C_2}{C_1 + C_2} \tag{C.5}$$

The expression (C.5) is used for the lower limit for C_{pto} in Section 2.2 and Section 2.3 as well as Chapter 5.